REPORT DOCUMENTATION PAGE

Form Approved
OMB NO. 0704-0188

1. AGENCY USE ONLY (Leave Blank)	2. REPORT DATE	3. REPORT TYPE AND DATES COVERED
	Nov-1998	FINAL 01 Sep 95 to 31 Aug 98

4. TITLE AND SUBTITLE

NARROWBAND AND MULTIPLE-ACCESS INTERFERENCE SUPPRESSION FOR DIRECT SEQUENCE SPREAD SPECTRUM COMMUNICATION RECEIVERS

5. FUNDING NUMBERS

DAAH04-95-1-0342
DAAG55-97-1-0389

6. AUTHOR(S)

John F. Doherty

7. PERFORMING ORGANIZATION NAME(S) AND ADDRESS(ES)
Iowa State Univerity, Ames, IA 50011
Pennsylvania State University, University Park, PA 16802

8. PERFORMING ORGANIZATION REPORT NUMBER

9. SPONSORING / MONITORING AGENCY NAME(S) AND ADDRESS(ES)

U. S. Army Research Office
P.O. Box 12211
Research Triangle Park, NC 27709-2211

10. SPONSORING / MONITORING AGENCY REPORT NUMBER

ARO 33481.4-MA-YIP
ARO 37800.1-MA-YIP

11. SUPPLEMENTARY NOTES

The views, opinions and/or findings contained in this report are those of the author(s) and should not be construed as an official Department of the Army position, policy or decision, unless so designated by the documentation.

12 a. DISTRIBUTION / AVAILABILITY STATEMENT
Approved for public release; distribution unlimited.

12 b. DISTRIBUTION CODE

13. ABSTRACT (Maximum 200 words)

This report presents research results focused on the mitigation of both narrowband and multiple-access interference in direct sequence spread spectrum communication systems. Both linear and nonlinear adaptive algorithmic approaches are developed and reported. Specific attention has been paid to making the algorithms practicable. In addition to the algorithmic development, a software simulation for a code-division multiple access system is developed using a commercially available programming environment.

14. SUBJECT TERMS
Spread Spectrum, CDMA, Interference Suppression

15. NUMBER OF PAGES
55

16. PRICE CODE

17. SECURITY CLASSIFICATION OF REPORT	18. SECURITY CLASSIFICATION ON THIS PAGE	19. SECURITY CLASSIFICATION OF ABSTRACT	20. LIMITATION OF ABSTRACT
UNCLASSIFIED	UNCLASSIFIED	UNCLASSIFIED	UL

Contents

List of Figures

List of Tables

Part I.

Statement of Problem Studied

The electromagnetic spectrum is an invaluable but limited natural resource for wireless communications. Increasing demands of military, commercial, and private users on the electromagnetic spectrum require an efficient spectrum channel sharing strategy. Static strategies, such as frequency-division multiple-accessing (FDMA) and time-division multiple-accessing (TDMA), by which the multiple-access channel is effectively partitioned into independent single-user subchannels, tend to be wasteful in applications where most users actively send information sporadically. Dynamic channel sharing strategies, which allow the active users a larger share of the channel while they are transmitting, fit into two categories: random-access communication and simultaneous transmission systems [1]. In random-access communication, it is assumed that the receiver cannot demodulate more than one simultaneous transmission, and so the problem is to design protocols to schedule channel access at non-overlapping times, and if collisions between messages occur to ensure that those messages are eventually retransmitted successfully. Simultaneous transmission systems differ from static strategies and random access protocols in that users are allowed to demodulate all (as in the satellite communications) or a subset (as in multipoint-to-multipoint topologies) of the transmitted messages.

A major multiple-access strategy using the simultaneous transmission philosophy is code-division multiple-accessing (CDMA) and it has become a main candidate for the next generation of mobile land and satellite communication systems. In CDMA communication systems, each transmitter generates a spread spectrum signal by modulating a data signal onto a pseudo-random signature waveform so that the resultant signal has a bandwidth much larger than the data signal bandwidth. Unlike frequency-division multiplexing (FDMA) or time-division multiplexing (TDMA), CDMA has multiple users simultaneously sharing the same wide-band channel. If a CDMA system is viewed in either the frequency or time domain, the multiple-access signals appear to co-exist.

The conventional CDMA receiver recovers the information of the desired user by correlating the received signal with a replica of the signature waveform assigned to the desired user, i.e., a signature matched filtering. As is well-known, when the received signal is corrupted by only additive white Gaussian noise (AWGN), the conventional matched filter receiver minimizes the error probability. This is not true in the conventional CDMA receiver, whose decision variables for the signal of a particular user are corrupted by *multiple-access interference* (MAI) in addition to AWGN. The MAI originates from cross-correlations between the signature waveform of the desired signal and signals of other active users. When the received signal power of the desired user is relatively weaker than those of the other users, the conventional receiver is unable to reliably recover the information sent by the desired user, even if the signature waveforms have very low cross-correlations. This is known as the *near-far problem* [2].

The current approach to dealing with the near-far problem is to use transmitter power control [3]. Another alternative is to use some form of a multi-user detector. Many different optimum/suboptimum structures of the multi-user detector have been proposed in the literature [2, 4–11]. Multi-user detectors are generally characterized by centralized detection that demodulates all the users' signals at the output of a matched filter bank. Substantial performance gains can be achieved in coherent multi-user systems by using a multi-user detector that takes advantage of the structure of the CDMA signals [2]. The multi-user detectors out perform the conventional receiver at the expense of a significant increase in complexity. For example, the complexity of the optimum multi-user detector in [2,4] grows exponentially in the number of users. Less complex suboptimum multi-user detectors in [5,6] linearly increase in complexity with the number of users. In addition to complexity, multi-user detectors also require large

amounts of side-information about the received signal, which includes the number of users, the signature waveforms, associated time delays, and phase offsets of all active CDMA signals. Often the received amplitude of each CDMA signal is also needed. The complexity of such multi-user detectors may be unacceptably high for many practical applications or communication security restrict the distribution of all users' signature waveforms to all the receivers, or both. Furthermore, some information of relatively weak signals is likely to be more difficult to obtain due to the time-varying nature of the channel.

This research investigated fully decentralized single-user detection, in which the receiver is constrained to demodulate the signal of only one user, but unlike the conventional receiver, is optimized to take into account the structure of the CDMA signal. The decentralized detection approach views the multi-user detection problem as an interference suppression problem, where at a particular receiver one signal is considered the desired signal and the other signals are considered the interference. One such single-user receiver is the linear minimum mean-squared-error (MMSE) receiver proposed in [12]. This MMSE receiver has been particularly attractive because it lends itself for adaptive implementation.

Several adaptive MMSE receivers have been proposed recently [12–14]. Although reducing the complexity and eliminating requirement of the information of the interfering signals, most of the adaptive MMSE receivers require training sequences for the implementation of the least-mean-square (LMS) algorithm both at the beginning and during data transmission. That is, adaptive MMSE receivers need to switch back and forth between a training mode and a decision-directed mode during actual data transmission as a new strong user accesses the system.

Use of a blind scheme, i.e., one that does not rely on a training sequence for adaptation, has been practically attractive for high-speed data transmission over a communication channel [15]. If the receiver yields a bit-error-rate (BER) less than 10^{-1} errors per bit, a decision-directed LMS algorithm may be an option for a blind receiver. However when the system experiences the near-far problem, detection capability of a non-optimum receiver is completely lost and the algorithm may suffer from the convergence to a local minimum associated with a strong interfering signal, i.e., the receiver may adapt its parameters to detect the signal of a strong interfering user instead of the signal of the desired user. Honig, Madhow and Verdu in [16] and Schodorf and Williams in [17] have proposed constrained output-power minimizing (OPM) receivers. They implement algorithms for a blind adaptive receiver through gradient projection (GP) algorithms. Algorithms in these receivers adjust the filter tap weights by minimizing the output power while constraining the gradient of the cost function to satisfy a prescribed constraint.

Part II.

Summary of Results

1. Blind Adaptive CDMA Receivers

1.1. Abstract

New blind adaptive interference suppression algorithms for DS/CDMA communication systems are developed. A generalized projection algorithm is developed that updates a multiple access interference (MAI) suppression filter in a static communication environment. The algorithm adaptively adjusts the filter coefficients by iteratively projecting them onto constraint sets. The constraint sets consist of data sets and property sets, which are obtained from the received signal and prior knowledge of the desired signal, respectively. A space alternating generalized projection algorithm with approximate EM mapping is also developed that suppresses MAI in a dynamic communication environment. This algorithm jointly estimates the filter and desired signal amplitude using a stochastic approximation of the EM algorithm. The performance results show that the new algorithms significantly out perform the existing adaptive algorithms in steady state.

1.2. Introduction

This research addresses the problem of data detection at system initialization. In such a case, the data estimates are not reliable during the initial adaptation process so that a decision-directed LMS-type algorithm is not feasible. An adaptive algorithm which does not rely on training data has been proposed in [18]. This algorithm implements a statistical gradient projection (GP) algorithm based on the output power minimization (OPM) criterion. The algorithm is considered *blind* since it does not incorporate any reference signal for the adaptation. However, it has been noted that the inclusion of the output power in the minimization process results in the signal cancellation phenomenon [19]. This phenomenon occurs when the performance measure does not asymptotically approach to zero. It is observed that the steady state performance of the algorithm in [18] does not approach the optimum and the algorithm requires switching from a blind mode to a decision-directed mode as soon as it converges, which is not practical in a dynamic communication environment.

For static communication, we develop a generalized projection algorithm that suppress the MAI. This algorithm assumes that the amplitude of the desired signal is known *a priori*. The algorithm minimizes a performance measure which does not involve training data and utilizes the amplitude as a reference signal. The algorithm adaptively adjusts the filter coefficients by iteratively projecting them onto some constraint sets. The constraint sets consist of the data set and the property set. The data set is used to specify that the response of the filter should be distortion-free with respect to the information sent by the desired user. The property set is used as a remedial measure which continually refines the filter coefficients in the direction of global convergence. It is obtained from the ideal convergence objective and some known property of the desired signal.

For dynamic communication, the amplitude of the desired signal may not be known *a priori* or it may vary with time. Therefore we develop a space alternating generalized projection algorithm with approximate EM mapping for the joint filter and amplitude

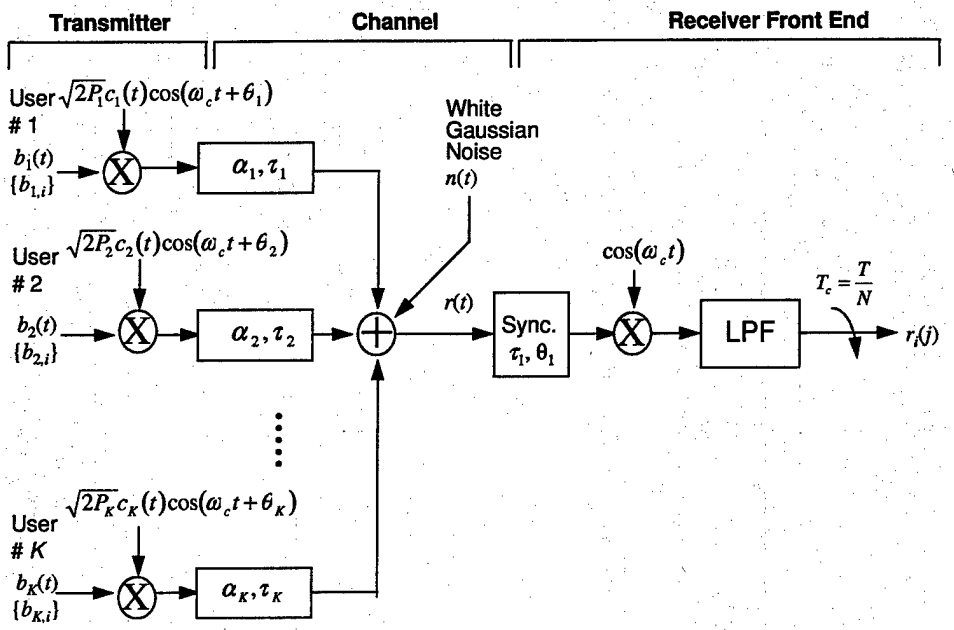

Figure 1.1.: A brief DS/CDMA system description

estimation. The algorithm is implemented by the combined application of a stochastic approximation of the EM algorithm [20] and the generalized projection algorithm. The algorithm decomposes the problem of estimating two unknown parameters into two decoupled parameter estimation problems. For each received signal, it iterates between estimating the conditional performance measure using the current received signal and the previous estimate of the parameters (E step), and minimizing the performance measure with respect to the unknown parameters (M step). In the M step of the algorithm, we minimize the conditional performance measure by iteratively projecting the parameters onto constraint sets.

1.3. System Description

The DS/CDMA system model considered is shown in Figure 1.1, where P_k, $b_k(t)$, $c_k(t)$ and θ_k are the transmitted power, data signal, signature waveform and phase offset of the kth user in the ith bit interval of duration T, respectively and ω_c is the common carrier frequency. The kth user's data signal is given by $b_k(t) = \sum_{i=-\infty}^{\infty} b_k(i)\,\varphi_T(t-iT)$, where $b_k(i) \in \{+1,-1\}$ is the ith data bit of the kth user and $\varphi_T(t)$ denotes the bit waveform with unity energy defined on $[0,T]$. Similarly, the kth user's signature waveform can be written as $c_k(t) = \sum_{n=0}^{N} c_k(n)\,\varphi_{T_c}(t-nT_c)$,where $c_k(n) \in \{+1,-1\}$ is the nth spreading code bit of the kth user, which has periodicity $N = T/T_c$ for all user k, and $\varphi_{T_c}(t)$ is the chip waveform with unity energy defined on $[0,T_c]$.

Without loss of generality, we assume that the signal of the first user ($k=1$) is the desired signal and the receiver is synchronized to this signal,(i.e., $\tau_1 = 0$ and $\theta_1 = 0$). The received signal at the ith bit interval can be described as an N-dimensional vector , which is given by

$$\mathbf{r}_i = A_1 b_1(i)\,\mathbf{c}_1 + \sum_{k=2}^{K} A_k\left[b_k(i-1)\,\mathbf{c}_k^L + b_k(i)\,\mathbf{c}_k^R\right] + \mathbf{n}_i \qquad (1.1)$$

Algorithm	Adaptation rule	Assumption
NLMS	$\mathbf{w}_{i+1} = \mathbf{w}_i - \mu\left(\mathbf{w}_i^T\mathbf{r}_i - d_i\right)\frac{\mathbf{r}_i}{\mathbf{r}_i^T\mathbf{r}_i}$	d_i is known
OPM-GP	$\mathbf{x}_{i+1} = \mathbf{x}_i - \mu\left(\mathbf{r}_i - \left[\mathbf{s}_1^T\mathbf{r}_i\right]\mathbf{s}_1\right)\frac{\mathbf{w}_i^T\mathbf{r}_i}{\mathbf{r}_i^T\mathbf{r}_i}$ $\mathbf{w}_{i+1} = \mathbf{s}_1 + \mathbf{x}_{i+1}$	$\mathbf{s}_1$ is known
Prop 1	$\mathbf{w}_{i,1} = T_R\mathbf{w}_i = \mathbf{w}_i - \mu\left(\left\|\mathbf{w}_i^T\mathbf{r}_i\right\| - A_1\right)\frac{\mathbf{r}_i}{\mathbf{r}_i^T\mathbf{r}_i}$ $\mathbf{w}_{i+1} = P_S\mathbf{w}_{i,1} = \left[1 - \mathbf{s}_1^T\mathbf{w}_{i,1}\right]\mathbf{s}_1 + \mathbf{w}_{i,1}$	A_1 and $\mathbf{s}_1$ are known
Prop 2	$\mathbf{w}_{i,1} = T_R\mathbf{w}_i = \mathbf{w}_i - \mu\left(\left\|\mathbf{w}_i^T\mathbf{r}_i\right\| - A_i\right)\frac{\mathbf{r}_i}{\mathbf{r}_i^T\mathbf{r}_i}$ $\mathbf{w}_{i+1} = P_S\mathbf{w}_{i,1} = \left[1 - \mathbf{s}_1^T\mathbf{w}_{i,1}\right]\mathbf{s}_1 + \mathbf{w}_{i,1}$ $A_{i+1} = A_i - \gamma\left[\left\|\mathbf{w}_i^T\mathbf{r}_i\right\| - A_i\right]$	$\mathbf{s}_1$ is known

Table 1.1.: Summary of adaptive algorithms

where $\mathbf{c}_k^L$ and $\mathbf{c}_k^R$ are the vectors related to the signature vector of the k^{th} user, $\mathbf{c}_k$, as $\mathbf{c}_k\left\lfloor l_k\right\rfloor = \mathbf{c}_k^L + \mathbf{c}_k^R$, $\mathbf{c}_k\left\lfloor l_k\right\rfloor$ is the cyclically shifted vector of $\mathbf{c}_k$ by l_k, and $\mathbf{n}_i$ is the noise vector with covariance matrix of $\sigma^2 I$. The related vectors are defined by

$$\begin{aligned}
\mathbf{r}_i &\triangleq \left[r_i(0), \cdots, r_i(N-1)\right]^T \\
\mathbf{c}_k &\triangleq \left[c_k(0), \cdots, c_k(N-1)\right]^T \\
\mathbf{c}_k^L &\triangleq \left[c_k(l_k), \cdots, c_k(N-1), 0, \cdots, 0\right]^T \\
\mathbf{c}_k^R &\triangleq \left[0, \cdots, 0, c_k(0), \cdots, c_k(l_k-1)\right]^T \\
\mathbf{n}_i &\triangleq \left[n_i(0), \cdots, n_i(N-1)\right]^T.
\end{aligned} \tag{1.2}$$

1.4. New Algorithm Development

In this research we develop two algorithms for determining the MAI rejection filter.

Generalized Projection Algorithm Utilize the received signal and some known properties of the desired signal to estimate the filter. Channel gain is assumed to be known.

Space Alternating Generalized Projection Algorithm with approximate EM Mapping Jointly and adaptively estimate the filter coefficients and the channel gain.

In Table 1.1, we summarize and compare four algorithms; the normalized LMS (NLMS), the normalized OPM-based gradient projection (OPM-GP), the generalized projection algorithm (Prop 1) and the space alternating generalized projection with approximate EM mapping algorithm (Prop 2).

Table 1.2 shows the computational complexity of the algorithms. It is assumed that all algorithms are synchronized to the desired signal and the filter length equals N. For fair comparison, we consider the normalized versions of the algorithms. It is seen that the added complexity in the implementation of the new algorithms is negligible.

1.5. Performance Results

In this section we demonstrate the performance of the new algorithms in a near-far situation. Our simulation results correspond to asynchronous communication systems in which the multiple access signals are modulated by 31-length Gold sequences. The

	NLMS	OPM-GP	Prop 1	Prop 2
Multiplication	$3N+3$	$5N+1$	$5N+2$	$5N+3$
Addition	$3N+1$	$6N$	$5N+2$	$5N+4$
$\lvert\cdot\rvert$	0	0	1	1
Storage requirement	$N+1$	$2N+1$	$2N+2$	$2N+3$

Table 1.2.: Computational complexity of the algorithms

ensemble-averaged output signal-to-interference ratio (SIR) at the ith iteration is obtained by

$$SIR_i = \frac{\sum_{m=1}^{M} \left(\mathbf{w}_{i,m}^T \mathbf{s}_1\right)^2}{\sum_{m=1}^{M} \left[\left(\mathbf{w}_{i,m}^T \mathbf{y}_{i,m}\right)/A_{1,m}\right]^2} \tag{1.3}$$

where $\mathbf{w}_{i,m}$ and $\mathbf{y}_{i,m} = \mathbf{r}_{i,m} - A_{1,m} b_{1,m} \mathbf{s}_1$ are the filter coefficients and the interference plus noise component of the received signal at the ith iteration in the mth realization, respectively. The number of realizations $M = 500$ is used to obtain the averaged output SIR. For each realization, the amplitudes, phase delays and the signature sequences of the signals are chosen randomly.

In Figure 1.2 and Figure 1.3, we simulate output SIR performances of the new algorithms and compare to the existing adaptive algorithms. In this simulation, the number of interferences is $(K-1) = 5$, the bit energy to background noise ratio (SNR) is 15 dB, and all interferences have amplitude 10 times greater than the amplitude of the desired signal, which accounts for the extreme near-far situation.

Figure 1.2 shows the output SIR curves of the generalized projection (Prop 1) algorithm, the OPM-based gradient projection (OPM-GP) algorithm of [18] and the normalized LMS (NLMS) algorithm in the training mode. The performance result shows that the Prop 1 algorithm converges to the steady state performance level similar to the NLMS algorithm in the training mode and improves about 5 dB in the steady state performance compared to the OPM-GP algorithm. The performance achievement of the Prop 1 algorithm is due to a performance criterion which asymptotically converges to zero, whereas the performance loss of the OPM-GP algorithm in the steady state is due to inclusion of the output power in the minimization process, which results in the signal cancellation phenomenon [19]. The slower convergence of the Prop 1 algorithm compared to the NLMS algorithm is explained by the fact that the former does not use training data for the adaptation whereas the latter does.

Figure 1.3 compares the space alternating generalized projection with approximate EM mapping (Prop 2) algorithm to the Prop 1 algorithm and the OPM-GP algorithm. For the Prop 2 algorithm, the forgetting factor in the amplitude estimation algorithm is $\gamma = 0.01$. It is shown that the steady state performance of the Prop 2 algorithm approaches that of the Prop 1 algorithm but is substantially better than that of the OPM-GP algorithm. The performance degradation of the Prop 2 algorithm over the Prop 1 algorithm is mainly caused by the amplitude estimation error, which can be reduced at the expense of convergence speed.

In Figure 1.4, we examine the steady state bit-error-rate (BER) performance of the new algorithms versus the input bit-energy to background noise ratio (SNR) and compare it to the matched filter, the NLMS algorithm in the decision-directed mode and the OPM-GP algorithm. In this simulation, simulation parameters are set equal to those used in Figure 1.2 and Figure 1.3 excepts the input SNR. A total of 2000 bits are transmitted for each realization and the last 1000 bits for 100 realizations are used to capture the steady state performance. The NLMS algorithm switches from

the training mode to the decision-directed mode after the 900th bit. It is evident that the performance of the Prop 1 algorithm is similar to the NLMS algorithm and approaches the single-user bound. The performance similarity between the Prop 1 algorithm and the NLMS algorithm in the high SNR range is due to the fact that both algorithms use performance criteria which converge close to zero. The performance of the Prop 2 algorithm is similar to the Prop 1 algorithm when the SNR is low and is slightly degraded over the Prop 2 algorithm as the SNR increases. These phenomena occur because the amplitude estimation error in the Prop 2 algorithm dominates the background noise in the high SNR range. It is also seen that the performance gains of the Prop 1 and Prop 2 algorithms over the OPM-GP algorithm increase when the SNR increases. In the OPM-GP algorithm the desired filter output and the background noise causes filter misadjustment whereas in the new algorithms only the background noise does. Interestingly, the performances of the Prop 1 and Prop 2 algorithms are slightly better than the NLMS algorithm when the SNR is lower than 6 dB. This shows that the decision-directed LMS algorithm is not feasible when the BER is higher than 10^{-1}.

The performance results demonstrate that the new algorithms are robust to decision errors and are nearly optimal without requiring training data. The performance results show the new algorithms are applicable for MAI suppression and information recovery in DS/CDMA communications.

1.6. Summary

We developed projection-based adaptive MAI suppression algorithms which require neither training data nor any information about the interfering signals. The algorithms are a generalized projection algorithm and a space alternating generalized projection algorithm with approximate EM mapping. The algorithms minimize the performance measure monotonically via the method of generalized projections and a stochastic approximation of the EM algorithm. The algorithms provide computationally efficient, robust, blind MAI suppression schemes when the near-far effect is predominant. Simulation results show that the new algorithms significantly improve the steady state performance over the OPM-GP based blind algorithm when the input SNR is higher than 3 dB. The new algorithms perform better than the NLMS algorithm when the input SNR is lower than 6 dB.

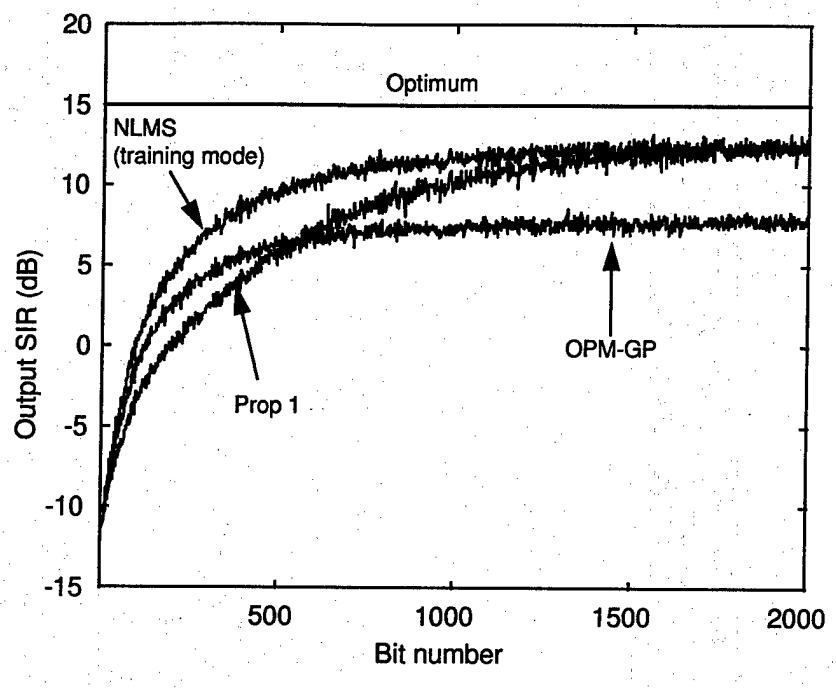

Figure 1.2.: Output SIR curves : $SNR = 15$ dB, $K = 6$, $\lambda = 0.2$, $A_k = 10A_1$, $k = 2, \cdots, K$.

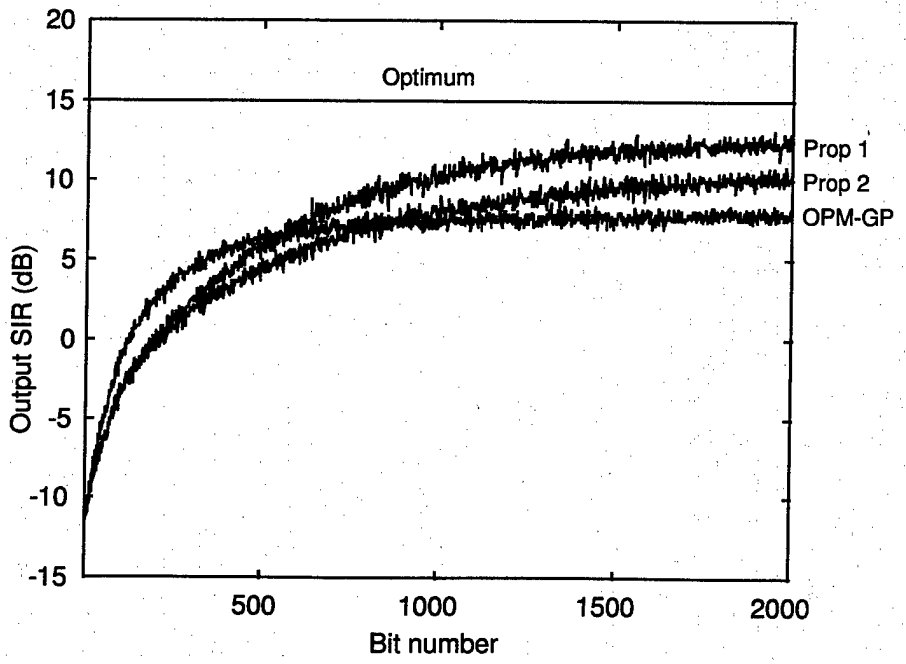

Figure 1.3.: Output SIR curves : $SNR = 15$ dB, $K = 6$, $\lambda = 0.2$, $\gamma = 0.01$, $A_k = 10A_1$, $k = 2, \cdots, K$.

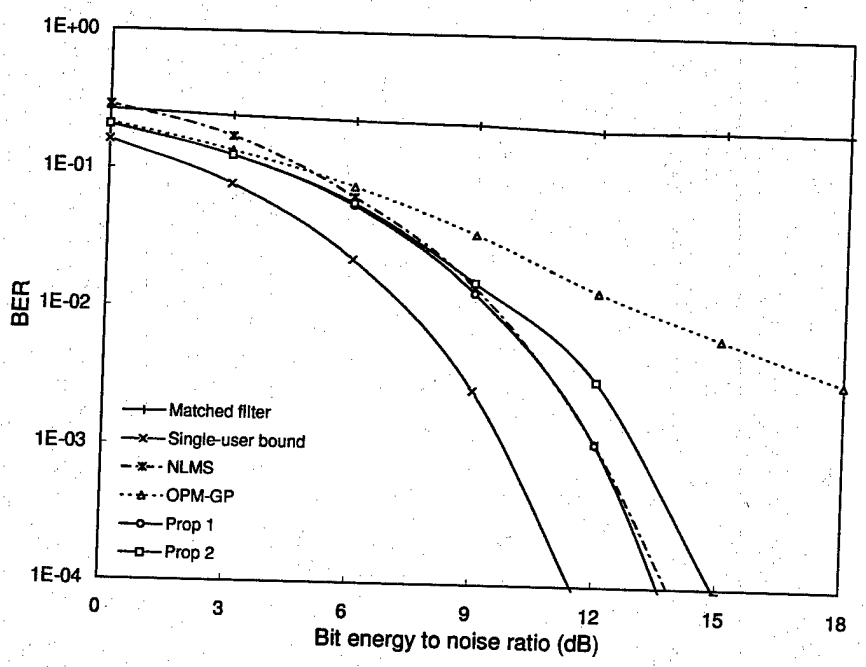

Figure 1.4.: Steady state BER performance : $K = 6$, $\lambda = 0.2$, $\gamma = 0.01$, $A_k = 10A_1$, $k = 2, \cdots, K$.

2. Decomposed Adaptive CDMA Receivers

2.1. Abstract

We develop a single-user decomposed adaptive receiver (DAR) structure for interference suppression in asynchronous direct-sequence code-division multiple-access (DS-CDMA) communication systems. Mathematical analysis and computer simulations show that the DAR has faster convergence than the conventional adaptive receivers with large processing gains in multiple access channel with additive white Gaussian noise.

2.2. Introduction

Among many sub-optimum interference suppression schemes for DS-CDMA systems the minimum mean squared error (MMSE) scheme has been an active research area due to its desired near-far resistance and direct applicability to adaptive implementation [21]. The MMSE adaptive receiver shows remarkable performance improvement over the conventional matched filter receiver [22, 23]. The main advantage of the adaptive receiver is that it can effectively suppress multiple access interference (MAI) without either the knowledge of interference parameters or the desired user's signature sequence by using a training sequence.

The N-tap MMSE adaptive receiver successfully removes asynchronous MAI when the number of users is much less than $N/2$, where N is the processing gain or the signature sequence length of the DS-CDMA system. In that case, however, the input to the conventional N-tap receiver is ill-conditioned in that the eigenvalue spread of input correlation matrix is very large. It is well known that the widely used least mean square (LMS) algorithm converges very slowly for ill-conditioned input data [24]. The slow convergence rate of LMS algorithm could be a serious limitation to system capacity and a deterrent to use MMSE receivers, especially when the channel is varying rapidly.

We develop a decomposed adaptive receiver (DAR) structure for single-user detection that has faster convergence characteristics than the conventional N-tap adaptive receiver. For the DAR, the N-tap adaptive receiver is decomposed into D smaller filters that are adapted individually. Coupling is used such that one filter's output is used for another filter's adaptation.

2.3. DS-CDMA System Model

We consider binary phase shift keyed (BPSK) asynchronous DS-CDMA system with signature sequence length N in an additive white Gaussian noise (AWGN) channel with noise power spectral density $N_o/2$. The received signal is modeled as

$$r(t) = \sum_{k=1}^{K} \sqrt{2P_k} c_k(t-\tau_k) b_k(t-\tau_k) \cos(\omega_o t + \theta_k) + n(t) \qquad (2.1)$$

where K is the number of users, P_k is the received power, $c_k(t)$ is the baseband bipolar signature waveform, $b_k(t)$ is the baseband bipolar waveform of data bit, $\tau_k \in [0, T)$

is the asynchronous timing offset, θ_k is the modulation phase offset of the k-th user respectively, and $n(t)$ the AWGN.

We assume that the received signal is demodulated to baseband, where it is processed by a normalized chip matched filter. The data from the chip matched filter for the i-th bit interval of the desired user is arranged as a vector,

$$\mathbf{r}(i) = \left[\begin{array}{cccc} r_1(i) & r_2(i) & \cdots & r_N(i) \end{array} \right]^T$$

We assume, without loss of generality, that the first user is the desired user and the receiver is synchronized to the first user, which yields [23]

$$\mathbf{r}(i) = b_1^{(i)}\mathbf{c}_1 + \sum_{k=2}^{K} b_k^{(i)} \sqrt{\frac{P_k}{P_1}} \cos(\theta_k)\mathbf{I}_k(i) + \mathbf{n}(i) \tag{2.2}$$

where $b_k^{(i)} \in \{-1, 1\}$ is the i-th bit of k-th user, $\mathbf{c}_1$ is the signature sequence vector of the desired user, $\mathbf{I}_k(i)$ is the interference vector from the asynchronous k-th user and $\mathbf{n}(i)$ is the Gaussian noise vector with zero mean and covariance matrix $\sigma^2\mathbf{I}$, where $\sigma^2 = N_o N/2E_b$ and E_b is the received energy per bit of the desired user.

2.4. Description Of Decomposed Adaptive Receiver

Let $\mathbf{w}(i) = \left[\begin{array}{cccc} w_1(i) & w_2(i) & \cdots & w_N(i) \end{array} \right]^T$ be the tap weight vector of the N-tap adaptive receiver and $y(i) = \mathbf{w}^T(i)\mathbf{r}(i)$ be the receiver output for i-th bit. Let N_j, $j = 1, 2, \cdots, D (D < N)$, be positive integers such that $\sum_{j=1}^{D} N_j = N$. Define $\mathbf{w}_j(i)$ as the j-th subfilter of $\mathbf{w}(i)$ of length N_j such that $\mathbf{w}(i) = \left[\begin{array}{cccc} \mathbf{w}_1^T(i) & \mathbf{w}_2^T(i) & \cdots & \mathbf{w}_D^T(i) \end{array} \right]^T$. Accordingly $\mathbf{r}(i)$ may be decomposed and represented as

$$\mathbf{r}(i) = \left[\begin{array}{cccc} \mathbf{r}_1^T(i) & \mathbf{r}_2^T(i) & \cdots & \mathbf{r}_D^T(i) \end{array} \right]^T.$$

It readily follows that the receiver output is $y(i) = \sum_{j=1}^{D} \mathbf{w}_j^T(i)\mathbf{r}_j(i)$.

Fig. 2.1 shows the structure of the DAR, where the outputs from the previous subfilters $\tilde{\mathbf{w}}_n(i)$, $n = 1, 2, \cdots, j-1$, are incorporated for the update of subfilter $\tilde{\mathbf{w}}_j(i)$. The length of the subfilter $\tilde{\mathbf{w}}_j(i)$ is the same as that of $\mathbf{w}_j(i)$. In this notation, $\tilde{\mathbf{w}}_j(i)$ is the value of the j-th subfilter using DAR adaptation and $\mathbf{w}_j(i)$ is the value obtained by conventional N-tap MMSE adaptation. The update equation for each subfilter $\tilde{\mathbf{w}}_j(i)$ is

$$\tilde{\mathbf{w}}_j(i+1) = \tilde{\mathbf{w}}_j(i) + \mu \left[s_j b_1^{(i)} - y_{j-1}(i) - \tilde{\mathbf{w}}_j^T(i)\mathbf{r}_j(i) \right] \mathbf{r}_j(i) \tag{2.3}$$

where $k_j = N_j/N$ is the ratio of the length of $\tilde{\mathbf{w}}_j(i)$ to that of $\mathbf{w}(i)$, $s_j = \sum_{n=1}^{j} k_n$, μ is the step size, $y_j(i) = \sum_{k=1}^{j} \tilde{\mathbf{w}}_k^T(i)\mathbf{r}_k(i)$ and $\tilde{d}_j(i) \equiv s_j b_j^{(i)} - \sum_{k=1}^{j-1} \tilde{\mathbf{w}}_k^T(i)\mathbf{r}_k(i)$. We note that $\tilde{d}_j(i) \approx k_j b_1^{(i)}$ when the accumulated outputs from the previous subfilters, $y_{j-1}(i)$, can successfully approximate $s_{j-1} b_1^{(1)}$ or $\tilde{\mathbf{w}}_n^T(i)\mathbf{r}_n(i) \approx k_n b_1^{(1)}$ for $n = 1, 2, \cdots, j-1$.

Each subfilter $\tilde{\mathbf{w}}_j(i)$ attempts to minimize the following mean squared error

$$\begin{aligned} & J_j\left(\tilde{\mathbf{w}}_j\right) \\ &= E\left[\left\{ s_j b_1^{(i)} - \sum_{k=1}^{j-1} \tilde{\mathbf{w}}_k^T(i)\mathbf{r}_k(i) - \tilde{\mathbf{w}}_j^T(i)\mathbf{r}_j(i) \right\}^2 \right] \\ &= E\left[\left\{ \tilde{d}_j(i) - \tilde{\mathbf{w}}_j^T(i)\mathbf{r}_j(i) \right\}^2 \right]. \end{aligned} \tag{2.4}$$

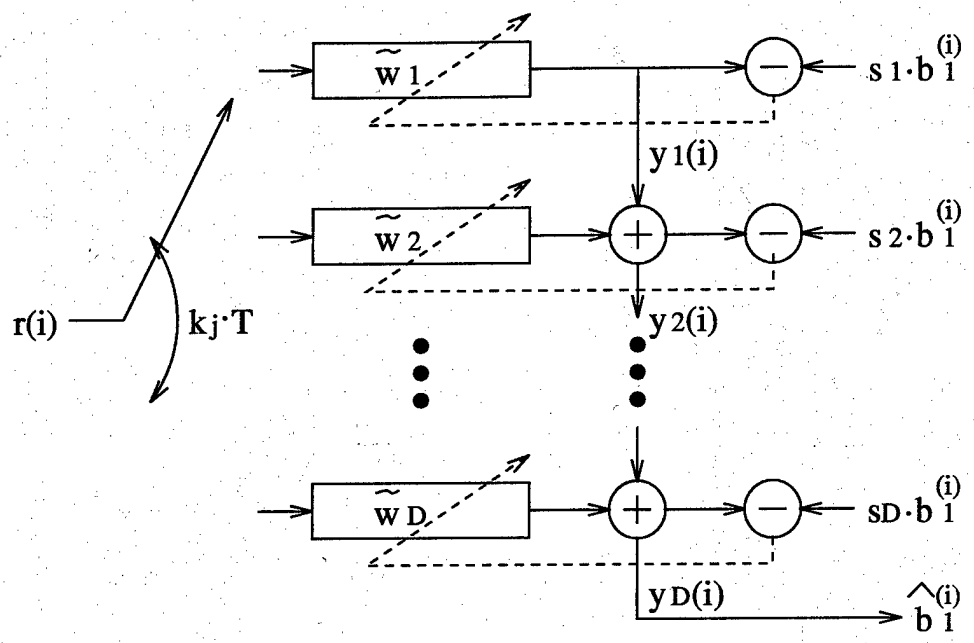

Figure 2.1.: Decomposed adaptive receiver

By comparison, the conventional N-tap MMSE adaptive receiver tries to minimize

$$J(\mathbf{w}) = E\left[\left\{b_1^{(i)} - \mathbf{w}^T(i)\mathbf{r}(i)\right\}^2\right]. \tag{2.5}$$

Using the decomposition described above $J(\mathbf{w})$ becomes

$$\begin{aligned} & J(\mathbf{w}) \\ &= E\left[\left\{b_1^{(i)} - \sum_{j=1}^{D} \mathbf{w}_j^T(i)\mathbf{r}_j(i)\right\}^2\right] \\ &= E\left[\left\{s_D b_1^{(i)} - \sum_{j=1}^{D-1} \mathbf{w}_j^T(i)\mathbf{r}_j(i) - \mathbf{w}_D^T(i)\mathbf{r}_D(i)\right\}^2\right] \\ &= E\left[\left\{d_D(i) - \mathbf{w}_D^T(i)\mathbf{r}_D(i)\right\}^2\right] \end{aligned} \tag{2.6}$$

where $d_D(i) \equiv s_D b_1^{(i)} - \sum_{j=1}^{D-1} \mathbf{w}_j^T(i)\mathbf{r}_j(i)$. Note that $J(\mathbf{w})$ in (2.6) is represented in the same way as $J_j(\tilde{\mathbf{w}}_j)$ in (2.4) for DAR, even though their minima may differ. Therefore, by employing the DAR, the N-tap MMSE problem with desired output $b_1^{(i)}$ is essentially transformed into an N_D-tap MMSE problem with desired output $d_D(i)$. This increases convergence performance since $N_D < N$.

If we assume that the input $\mathbf{r}(i)$ is a stationary vector process, the correlation matrix $\mathbf{R}_{DD} = E\left[\mathbf{r}_D(i)\mathbf{r}_D^T(i)\right]$ is submatrix of correlation matrix $\mathbf{R} = E\left[\mathbf{r}(i)\mathbf{r}^T(i)\right]$. Then from the Cauchy interlacing theorem [25] it is guaranteed that the eigenvalue spread of $\mathbf{R}_{DD}$ is less than or equal to the eigenvalue spread of $\mathbf{R}$. Since the convergence rate of the LMS algorithm depends on the eigenvalue spread of the input data correlation matrix, the DAR has a faster convergence rate than the N-tap adaptive

receiver. Even in the case that the eigenvalue spread of $\mathbf{R}_{DD}$ is the same as that of $\mathbf{R}$, we still expect that DAR converges faster since the length of $\tilde{\mathbf{w}}_D(i)$ is shorter than that of $\mathbf{w}(i)$ and the convergence rate is inversely proportional to the adaptive filter length [24].

From (2.4), D normal equations are obtained for each subfilter $\tilde{\mathbf{w}}_j(i)$ that are combined into one matrix equation as follows.

$$\begin{bmatrix} \mathbf{R}_{11} & \mathbf{0} & \cdots & \mathbf{0} \\ \mathbf{R}_{21} & \mathbf{R}_{22} & \ddots & \vdots \\ \vdots & \vdots & \ddots & \mathbf{0} \\ \mathbf{R}_{D1} & \mathbf{R}_{D2} & \cdots & \mathbf{R}_{DD} \end{bmatrix} \begin{bmatrix} \tilde{\mathbf{w}}_{o1} \\ \tilde{\mathbf{w}}_{o2} \\ \vdots \\ \tilde{\mathbf{w}}_{oD} \end{bmatrix} = \begin{bmatrix} s_1\mathbf{p}_1 \\ s_2\mathbf{p}_2 \\ \vdots \\ s_D\mathbf{p}_D \end{bmatrix} \tag{2.7}$$

where $\mathbf{R}_{jk} = E\left[\mathbf{r}_j(i)\mathbf{r}_k^T(i)\right]$, $\mathbf{p}_j = E\left[b_1^{(i)}\mathbf{r}_j(i)\right]$, and $\tilde{\mathbf{w}}_{oj}$ is the Wiener solution for subfilter $\tilde{\mathbf{w}}_j(i)$, $j,k = 1,2,\cdots,D$. It is interesting to compare (2.7) with the following N-tap normal equation expressed in block decomposed form,

$$\begin{bmatrix} \mathbf{R}_{11} & \mathbf{R}_{12} & \cdots & \mathbf{R}_{1D} \\ \mathbf{R}_{21} & \mathbf{R}_{22} & \ddots & \vdots \\ \vdots & \vdots & \ddots & \mathbf{R}_{D-1D} \\ \mathbf{R}_{D1} & \mathbf{R}_{D2} & \cdots & \mathbf{R}_{DD} \end{bmatrix} \begin{bmatrix} \mathbf{w}_{o1} \\ \mathbf{w}_{o2} \\ \vdots \\ \mathbf{w}_{oD} \end{bmatrix} = \begin{bmatrix} \mathbf{p}_1 \\ \mathbf{p}_2 \\ \vdots \\ \mathbf{p}_D \end{bmatrix} \tag{2.8}$$

where $\mathbf{w}_{oj}$ is the j-th subvector of the N-tap optimum Wiener solution [24]. In (2.7) the upper block triangular part of the original correlation matrix is removed and the original cross-correlation vector is scaled block by block to compensate.

2.5. Performance Results

In our computer simulations 1000 bits are transmitted with $E_b/N_o = 10dB$. The signature sequences are Gold codes of length $N = 127$ and are assigned to 50 asynchronous users. We assume a near-far situation where $P_k/P_1 = 10$, in (2.2), for 10 of the 50 users and $P_k/P_1 = 1$ for the remaining users. The step size of the LMS algorithm for any filter is set to 0.5% of $2/\lambda_{max}$, where λ_{max} is the maximum eigenvalue of input correlation matrix for that filter. We compare the MSE performance of DAR-2 and DAR-4 with that of the N-tap conventional receiver, where DAR-n refers to DAR obtained by decomposing the N-tap receiver into n sections. We simulate the cases where DAR-n has $n-1$ subfilters of length $(N+1)/n$ taps followed by a subfilter of length $(N+1)/n - 1$ taps.

Fig. 2.2 shows the MSE plots obtained by averaging 500 trials, which shows that DAR-2 and DAR-4 converge faster than the N-tap receiver. Furthermore, DAR-4 converges faster than DAR-2, which confirms the mathematical reasoning given in Section 2.4. Fig. 2.3 presents the adaptive filter tap error norm (2-norm) with respect to the Wiener solution of the N-tap filter. The overall tap weight vectors of DAR-2 and DAR-4 converge faster toward the Wiener solution, but also saturate earlier. It is expected that the DAR has a larger steady state MSE than the N-tap adaptive receiver. There is a trade-off between the steady state MSE and the convergence rate of the DAR controlled by parameter D, i.e., the number of subfilters. Under a rapidly changing channel condition, the DAR could reach the system state for reliable communication faster while incurring an increase in steady state error. Under such conditions, its overall performance is better than that of the conventional N-tap adaptive receiver for moderate values of the parameter D.

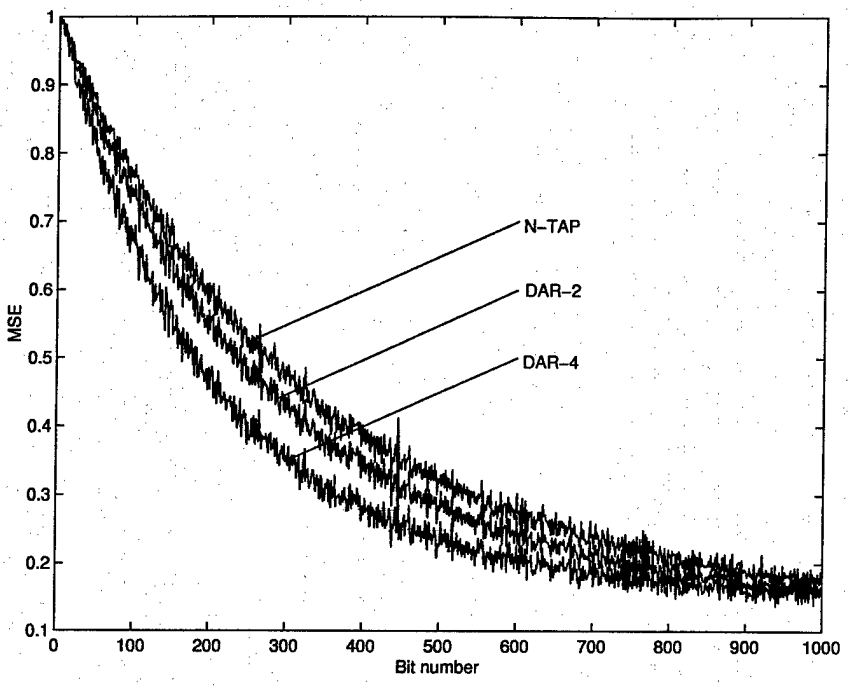

Figure 2.2.: MSE of LMS algorithm, N=127, K=50 with 10 stronger($10dB$) interferers

2.6. Summary

In this research we developed a decomposed adaptive receiver (DAR) for DS-CDMA systems. Mathematical analysis of MMSE for the DAR was given to show the faster convergence characteristics of DAR. In computer simulations the DAR scheme showed improved convergence performance in both MSE and tap weight error norm.

Since the capacity of DS-CDMA systems and the convergence rate of an adaptive receiver depend on the processing gain in a conflicting manner, it is advantageous to have an adaptive receiver structure with a faster convergence rate. The DAR structure developed in this research could increase the capacity of DS-CDMA systems to a considerable extent by making adaptive receivers practical for systems with large processing gains.

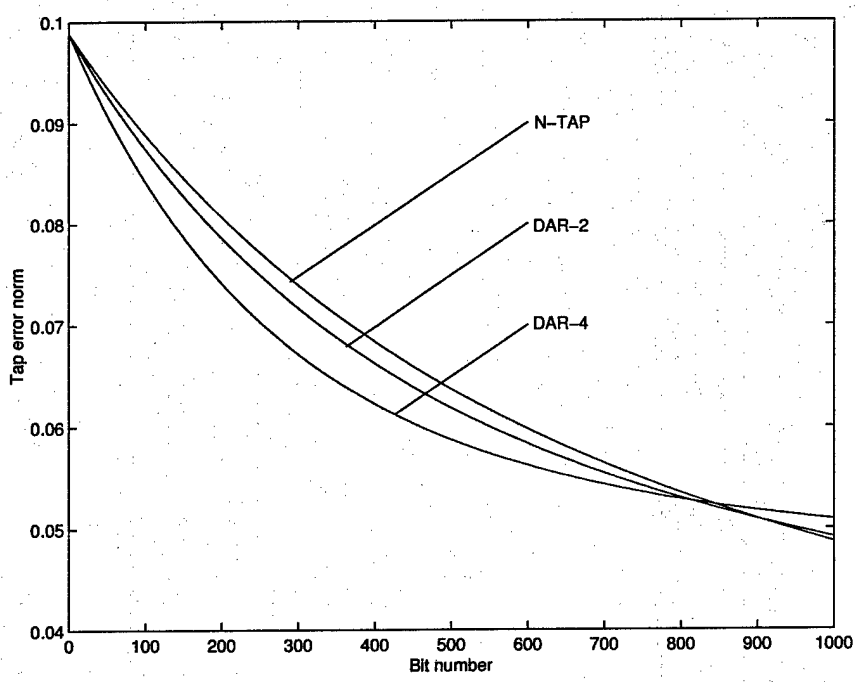

Figure 2.3.: Tap error norm of LMS algorithm, N=127, K=50 with 10 stronger($10dB$) interferers

3. Block Iterative CDMA Receiver

3.1. Abstract

An interference suppression scheme using a block iterative algorithm, row-action projection (RAP) algorithm for direct- sequence spread-spectrum (DS/SS) code-division multiple-access (CDMA) systems is developed. The performance results for the near-far problem and the interference increments due to increasing co-channel users using RAP algorithm are compared with normalized least mean square (NLMS) algorithm. It is concluded that RAP algorithm can improve the convergence rate of NLMS algorithm and is a practical alternative to the NLMS or LMS interference rejecter.

3.2. Introduction

The goal of using spread spectrum is to substantially increase the bandwidth of an information-bearing signal beyond that needed for basic communications. The bandwidth increase, while not necessary for communication, can mitigate the harmful effects of interference. Interference mitigation is a well-known property of all spread spectrum systems [43]. However, the interfering signal is often so powerful so that the communication becomes effectively impossible. For example, the crosscorrelations between the spreading sequences for different transmissions are nonzero, thus, increasing co-channel users can disrupt the reception of desired signal. Another problem is that nearby interferers raise the detection difficulty for highly attenuated desired signals, known as near-far effect. Immunity to such interference can be improved significantly by using signal processing techniques [44]. Interference suppression schemes are typically based on the minimum mean squared error (MMSE) criterion. Adaptive estimation schemes are widely used in this problem, in which the standard algorithm is the least-mean-square (LMS) algorithm [45]. The advantage of LMS algorithm as compared to other algorithms is its low complexity in computation. The LMS algorithm produces an approximation to the minimum mean square error estimate; the expected value of the output error square approaches zero. The major drawback of the LMS algorithm is that its convergence rate is dependent upon the eigenvalue spread of the input data correlation matrix. Thus, the LMS algorithm may be excluded from high-speed, real-time signal processing applications. A block iterative algorithm, row-action projection (RAP) algorithm [46] can offer the same low computation complexity as LMS algorithm with an improved convergence rate. The RAP algorithm performs coefficient updates by using the data matrix more than once. It offers O(N) complexity, easy implementation, stable operation and improved convergence rate. In this research, the RAP algorithm is applied to multiple-access interference suppression in CDMA receiver.

3.3. System Model and Problem Formulation

The received signal is the sum of K simultaneous CDMA transmissions plus additive white Gaussian noise. The normalized baseband signal in a carrier-synchronous system

due to the jth user is given by [12]

$$r_j(t) = \sum_{t=-\infty}^{\infty} b_{i,j} \sum_{k=0}^{N-1} a_j[k]\psi(t - iT - \nu_j - kT_c) \tag{3.1}$$

for $1 \leq j \leq K$, where T is the bit interval, $b_{i,j} \in \{1, -1\}$ is the i^{th} bit of the j^{th} user, ν_j is the delay of the j^{th} user, $\sum_{k=0}^{N-1} a_j[k]\psi(t - kT_c)$ is the spreading waveform, $a_j[k] \in \{1, -1\}$ is the k^{th} element of the spreading sequence for the j^{th} user, N is the processing gain, and $\psi(t)$ is the chip waveform with unit energy and duration $T_c = T/N$. It is assumed that the receiver is synchronized to the desired transmission and the delay of the desired user is $\nu_1 = 0$. For $2 \leq j \leq K$ the relative delay $\nu_j = (\tau_j + \delta_j)T_c$ where τ_j is an integer normally distributed between 0 and $N - 1$ and δ_j is normally distributed in the interval $[0, 1)$. It is assumed that the received transmissions are chip synchronized which gives $\delta_j = 0$. The discrete-time equivalent model for the received signal is now [12]:

$$r = b_{0,1}a_1 + \sum_{j=2}^{K} \sqrt{P_j}(b_{0,j}a_{0,j} + b_{-1,j}a_{-1,j}) + n \tag{3.2}$$

where $a_j = (a_j[0], a_j[1], \cdots, a_j[N-1])^T$, $[a_{0,j}]_k = a_j[k - \tau_j]$, $[a_{-1,j}]_k = a_j[k + N - \tau_j]$, for $0 \leq k \leq N - 1$ and $2 \leq j \leq K$, and $a_j[m] = 0$ for $m < 0$. The white noise vector n is Gaussian with mean zero and covariance matrix $\sigma^2 I_N$, where I_N denotes the $N \times N$ identity matrix and $\sigma^2 = N_0/2$. The interference suppression problem is now formulated as:

$$\begin{bmatrix} d_i \\ d_{i-1} \\ \vdots \\ d_{i-L+1} \end{bmatrix} = \begin{bmatrix} r_i^T \\ r_{i-1}^T \\ \vdots \\ r_{i-L+1}^T \end{bmatrix} \begin{bmatrix} c_{0,i} \\ c_{1,i} \\ \vdots \\ c_{N-1,i} \end{bmatrix} + \begin{bmatrix} e_i \\ e_{i-1} \\ \vdots \\ e_{i-L+1} \end{bmatrix} \tag{3.3}$$

In compact notation, $d = Xc + e$, where d represents the bit sequence that is transmitted, X is the state matrix of the received signal, c is the unknown filter coefficient vector and e is the residual error of the estimation process. The parameter L denotes the processing block size.

3.4. Row-Action Projection (RAP) Algorithm

In (3.3), each equation describes a hyperplane in the coefficient space. If the set of equations is consistent, there will be only one solution vector that satisfies all the hyperplanes. The optimal solution for noiseless data satisfies all the equations exactly, implying that all the hyperplanes share a common point. The presence of noise perturbs the hyperplanes from the common point. An optimal coefficient vector that terminates at a point whose distance from each hyperplane is minimized under certain criterion can be found. The point with minimum sum of squared distances (least-squares) is a typical optimality criterion. The goal of the RAP algorithm is to attain this optimal solution via a sequence of orthogonal projections toward the hyperplanes. The projection of an arbitrary solution vector onto a hyperplane is accomplished by

$$c_{i+1} = c_i + \mu[d_j - c_i^T r_j]\frac{r_j}{\|r_j\|^2} \tag{3.4}$$

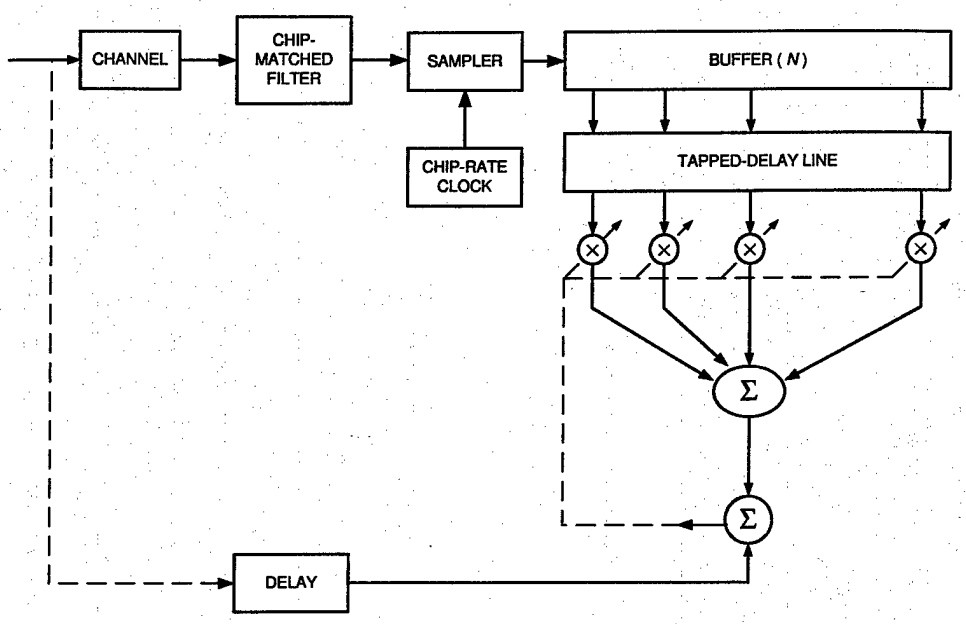

Figure 3.1.: The adaptive filter used for interference rejection. The reference signal is delayed to center the impulse response of the adaptive filter. The tapped-delay line was loaded every N chip interval.

where c_i is the previous estimate and c_{i+1} is the updated estimate that, if $\mu = 1$, exactly satisfies the j^{th} equation in (3.3). The iteration index related to the equation index by $j = i \ mod \ l$. The basic operation of RAP algorithm [46] is to sequentially apply (3.4) on the equations in (3.3) repeatedly. The first step is to store the data vector along with desired output in the buffer. Once the data buffer is full, the second step is to make multiple updates of the adaptive coefficients by sequentially using the data and the update equation (3.4). After finishing the desired updates with current data, the next step is to obtain new data vector from data buffer and repeat the updating process.

3.5. Performance Results

This section presents the performance results obtained for the RAP algorithm applied to an interference rejecter in a DS/SS CDMA system. The RAP algorithm is contrasted to the NLMS algorithm to compare the convergence rate and the steady state output SNR. The interference rejecter is implemented using a transversal filter structure, as shown in Figure 3.1. The adaptive filter length is the same as the chip number of each information bit. The chip number was 31 in the simulation. The step size used in the simulation for both RAP and NLMS algorithm is the same, which was 0.05. The SNR of the received signal, which is fed into the chip-matched filter, is 10 dB per bit. The channel characteristics and the interference characteristics are unchanged during each simulation run. The output SNR is defined as the ratio of the mean square to the variance of the interference rejecter output [47]. There are 50 different ensembles in each simulation. The output SNR converges throughout the process. In order to measure the convergence rate and the steady state output SNR, the function, $f(t)$, is

used to model the output SNR (dB) curve where the function is defined as:

$$f(t) = -(A - B)e^{(-t/\tau)} - B \tag{3.5}$$

where t is the time (bits), τ is the time constant, a measurement of convergence rate, and $-B$ is the steady state output SNR (dB). A , B , and τ are found in the least square error sense. The performance of both RAP and NLMS algorithm for near-far scenario is shown in Figure 3.2. The near-far scenario is quantified by the near-far parameter NF, which indicates the number of users whose power level is ten times the power level of the desired user. In this part of simulation, the total number of users is ten. For instance, for NF=3 there are three users whose power level is ten times the desired users power level and seven users, including the desired user, whose power level is the same as the desired users power level. The processing block size is 4 bits. In the performance result shown in Figure 3.2, RAP algorithm provides a better convergence rate while two or more iterations are performed. In the case where three iterations are performed, the convergence rate is 2.3 times faster than the convergence rate provided by NLMS algorithm. Meanwhile, the performance result demonstrates that with proper iteration numbers, the output SNR of RAP algorithm stays close to the level provided by NLMS algorithm. More iteration performed on each data block will produce faster convergence but the output SNR will decrease. For example, performing ten iterations on each data block yields a convergence rate that is 4.3 times faster than NLMS algorithm on average and a output SNR that is degraded by 0.72 dB on average. Theoretically, there are $N + 2$ users allowed in a CDMA system with the length N spreading code. Due to the non-zero property of the cross correlation function of spreading code, increasing the user number will raise the interference power and downgrade the system performance. The performance of RAP and NLMS algorithm for the interference increment problem due to additional users was shown in Figure 3.3. In this part of simulation, every user was set at the same power level as the desired users power level. With the proper iteration number, for example, three iterations, the convergence rate is 1.6 times faster than the convergence rate provided by NLMS algorithm on average. With the proper iteration number, the output SNR by RAP algorithm kept at the same level as NLMS algorithm. In the case of performing ten iterations, the convergence rate is 3.4 times faster on average and the output SNR is degraded by 0.64 dB on average.

3.6. Summary

In this research, an interference suppression scheme using the RAP algorithm for DS/SS CDMA system is developed. The RAP algorithm achieves $O(N)$ complexity by iteratively operating on the rows of the data matrix individually to form updates of the unknown adaptive coefficients. The RAP performs multiple update in the same set of data. The convergence rate of RAP algorithm is better than NLMS algorithm, especially at times that the near-far effect is severe, when the processing block size is properly chosen. With proper iteration number, the RAP algorithm provides the same output SNR level with NLMS algorithm while the convergence rate is well improved. The computation and memory needs are increased due to data buffering and multiple update. In the performance result, a proper choice of iteration number and block size, for instance, three iterations and 4 bits per processing block, will need triple the computation and four times the memory comparing to NLMS algorithm. In the system that is able to afford the computation and memory increment, the RAP algorithm is an alternative interference suppression scheme which provides better convergence rate and the same output SNR level as the LMS algorithm.

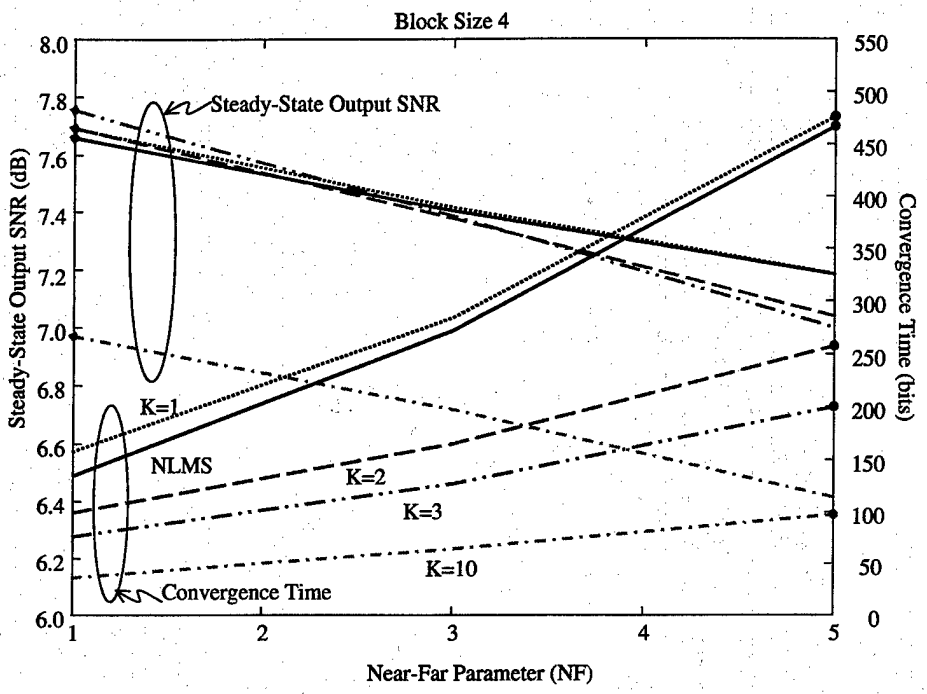

Figure 3.2.: The performance of RAP algorithm for near-far problem in contrast with NLMS algorithm. K is the iteration number.

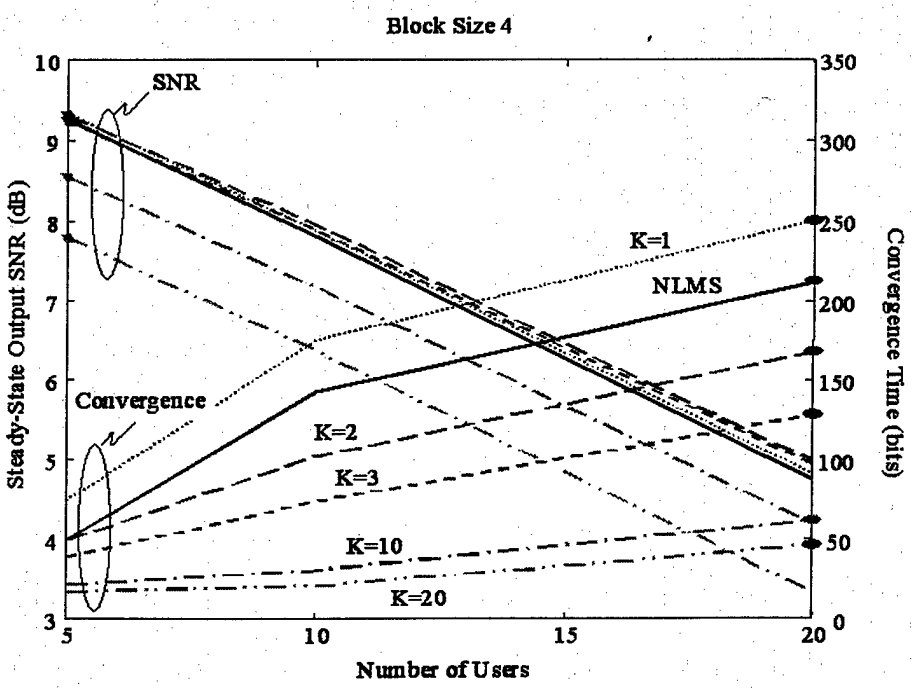

Figure 3.3.: The performance of RAP for the interference due to the increasing co-channel users. K is the iteration number.

4. Regularized Narrowband Interference Suppression in CDMA Systems

4.1. Abstract

A regularized LMS technique is presented that uses a modified optimality criterion which enhances the detection capabilities of direct sequence spread spectrum systems. The rejection filter is updated based upon an additional regularization input which limits the self-noise of the filter, especially at moderate signal-to-interference power ratios. The regularization is controlled by a single scalar parameter, that can be varied to produce the optimal Wiener filter weights or the decision-feedback filter weights. An advantage of the regularized filter is that the weight error surface is quadratic, leading to well behaved convergence properties for adaptive implementations. performance results are presented which compare the regularized filter to the optimal Wiener filter and the decision-feedback filter.

4.2. Introduction

Discrete-time adaptive linear rejection filtering of narrowband interference can improve the performance of direct sequence spread spectrum (DS/SS) systems [26,27]. In these results, the discrete-time (coherently) received signal is modeled by

$$z(n) = I_{\lfloor n/L \rfloor} c(n) + j(n) + v(n) \tag{4.1}$$

where the information bit takes on the values $I_n = \pm 1$ with equal probability, $c(n)$ is the chip sequence, $j(n)$ is the jamming signal, $v(n)$ is thermal (white) noise, L is the number of chips per bit, and $\lfloor x \rfloor$ is the greatest integer less than or equal to x. The sampling period is T_c seconds, or once per chip interval. It is possible to predict the jammer using Wiener filtering because the dominant correlation in $z(n)$ is due to $j(n)$. The jammer is removed by subtracting the prediction from the received signal

$$e(n) = z(n) - \sum_{l=1}^{N} w_l^K x(n - l - K) \tag{4.2}$$

where $e(n)$ is the error process which estimates the DS/SS signal $s(n) = I_{\lfloor n/L \rfloor} c(n)$, $x(n)$ is the prediction filter input, and $K \geq 0$ sets the minimum prediction delay. The rejection filter coefficients $\mathbf{w}^K = \left[w_1^K w_2^K \ldots w_N^K\right]^T$ are usually designed to satisfy the minimum mean square error optimality criterion, and thus are the solution to the Wiener-Hopf equations [28]

$$\mathbf{R}_{\mathbf{xx}}^K \mathbf{w}^K = \mathbf{p}_{dx}^K \tag{4.3}$$

where the input autocorrelation matrix is

$$\mathbf{R}_{\mathbf{xx}} \triangleq \mathrm{E}\left\{\mathbf{x}_n^K \left[\mathbf{x}_n^K\right]^T\right\} \tag{4.4}$$

and the elements of the cross-correlation vector are

$$\left[\mathbf{p}_{\mathbf{dx}}^K\right]_i \triangleq \rho_{d\mathbf{x}}(i+K) \triangleq \mathrm{E}\left\{d(n)\left[\mathbf{x}_n^K\right]_i\right\} = \mathrm{E}\left\{d(n)x(n-i-K)\right\} \tag{4.5}$$

For notation, let (4.4) define the autocorrelation matrix for any vector, e.g., $\mathbf{a}$ has autocorrelation matrix $\mathbf{R_{aa}}$. Likewise, the cross-correlation vector between a scalar a and a vector $\mathbf{b}^K$ is $\mathbf{p}^K_{\mathbf{ab}}$, as defined by (4.5).

The filter weights obtained according to (4.3) will form an estimate of the desired signal $d(n)$ based upon the filter input vectors

$$\mathbf{x}_n^K = [x(n-1-K)x(n-2-K)\ldots x(n-N-K)]^T .$$

The optimal desired signal for the prediction filter output is $d(n) = j(n) + v(n)$, which yields $e(n) = s(n)$. The optimal cross-correlation vector becomes

$$\mathbf{p}^K_{\mathbf{dx}} = \mathbf{p}^K_{\mathbf{jx}} = \mathbf{p}^K_{\mathbf{jj}} \tag{4.6}$$

assuming $x(n) = z(n)$ and assuming mutually uncorrelated signal components. The desired signal typically used in (4.2) is the received signal, which produces the cross-correlation vector

$$\mathbf{p}^K_{\mathbf{dx}} = \mathbf{p}^K_{\mathbf{jx}} + \mathbf{p}^K_{\mathbf{sx}} = \mathbf{p}^K_{\mathbf{jj}} + \mathbf{p}^K_{\mathbf{ss}} \tag{4.7}$$

It is usually assumed that the DS/SS signal is perfectly uncorrelated, i.e., $\mathbf{p}^K_{\mathbf{ss}} = 0$, in which case (4.6) and (4.7) are identical. Thus, an estimate of the optimal filter can be obtained from solving [29]

$$[\mathbf{R_{jj}} + \mathbf{R_{ss}} + \mathbf{R_{vv}}]\,\mathbf{w}^0_{WF'} = \mathbf{p}^0_{\mathbf{jj}} + \mathbf{p}^0_{\mathbf{ss}} \tag{4.8}$$

where $\mathbf{R_{xx}} = \mathbf{R_{jj}} + \mathbf{R_{ss}} + \mathbf{R_{vv}}$. The subscript on the filter tap-weight vector signifies the filter type for the remainder of the report.

It has been recognized that the presence of the DS/SS signal $s(n)$ at the prediction filter input induces distortion of the DS/SS signal, resulting in a reduced correlation peak and reduced immunity to noise [26]. This is evident when (4.2) is decomposed into it constituent parts

$$e(n) = \left[s(n) - \sum_{l=1}^{N} w_l^K s(n-l-K)\right] + \left[j(n) - \sum_{l=1}^{N} w_l^K j(n-l-K)\right] + v'(n) \tag{4.9}$$

where $v'(n)$ is the filtered thermal noise. The first term on the right-hand-side is the "self-noise" of the rejection filter and is due to the filtering of the DS/SS signal. One technique to reduce the filter self-noise is to remove the DS/SS signal from the filter input by using decision-feedback filtering [26,30]. This corresponds to a filter input

$$x_{DF}(n) = z(n) - \hat{I}_{\lfloor n/L \rfloor} c(n) = \left(I_{\lfloor n/L \rfloor} - \hat{I}_{\lfloor n/L \rfloor}\right) c(n) + j(n) + v(n) \tag{4.10}$$

where $\hat{I}_{\lfloor n/L \rfloor}$ is the estimated bit. Assuming perfect feedback, $I_{\lfloor n/L \rfloor} = \hat{I}_{\lfloor n/L \rfloor}$, then the prediction filter output is

$$e_{DF}(n) = s(n) + \left[j(n) - \sum_{l=1}^{N} w^K_{DF_l} s(n-l-K)\right] + v'(n) \tag{4.11}$$

where $K \geq L$ to ensure causality of the estimates $\hat{I}_{\lfloor n/L \rfloor}$. Assuming that $K = L$, the filter weights in (4.11) are given by

$$[\mathbf{R_{jj}} + \mathbf{R_{vv}}]\,\mathbf{w}^L_{DF} = \mathbf{p}^L_{\mathbf{jj}} \tag{4.12}$$

The result in (4.12) can be viewed as an augmentation of the optimal linear predictive filter

$$[\mathbf{R_{jj}} + \mathbf{R_{ss}} + \mathbf{R_{vv}}]\,\mathbf{w}^L_{WF_{opt}} = \mathbf{p}^L_{\mathbf{jj}} \tag{4.13}$$

where the DS/SS signal autocorrelation matrix $\mathbf{R_{ss}}$ has been removed from the left-hand-side of (4.13). One major difference between the two filters is that the DS/SS signal does not pass through the decision-feedback filter. Another difference concerns the adaptive implementation of the decision-feedback filter. The adaptive filter weights for the Wiener filter converge monotonically to a unique local minimum of the weight error surface. By comparison, the convergence of the adaptive decision-feedback filter is problematic due to the multiple local minima introduced into the error surface by the non-linear decision element.

The analysis of the adaptive performance of transversal rejection filters, as in (4.2), has been well documented [31–34]. Other interference rejection approaches are also viable, such as lattice filters [35], transform domain filters [36], and nonlinear processing [37–39].

In this research, we consider transversal rejection filters and extend the concept of autocorrelation matrix augmentation to include modifications of the form

$$[\mathbf{R_{jj}} + \mathbf{R_{ss}} + \mathbf{R_{vv}} - \beta\mathbf{R_{rr}}]\,\mathbf{w}^K_\beta = \mathbf{p}^K_{\mathbf{jj}} \tag{4.14}$$

which will be termed regularization. The regularization of the solution is controlled by the matrix $\mathbf{R_{rr}}$ and scalar β. We see that the decision feedback filter in (4.12) uses the regularization matrix $\mathbf{R_{ss}}$ and the regularization parameter $\beta = 1$.

4.3. Adaptive Regularized Interference Rejection

In the typical interference rejection techniques, the desired signal is a delayed version of the input, which is composed of the interference signal, DS/SS signal, and thermal noise. Ideally, the desired signal should be independent of the DS/SS signal to negate any correlation canceling caused by the rejection filter. To approach this goal, we regularize the standard LMS rejection filter update, incorporating information regarding the DS/SS signal correlation. Assuming a predictor form for the rejection filter, the regularized LMS update is given by

$$\mathbf{w}_{n+1} = \mathbf{w}_n + \mu\left[x(n) - r(n) - \mathbf{w}_n^T\left(\mathbf{x}^0_n - \beta\mathbf{r}^0_n\right)\right]\left[\mathbf{x}^0_n + \mathbf{r}^0_n\right] \tag{4.15}$$

where $r(n)$ is the regularization input and $x(n) = s(n)+j(n)+v(n)$ is the DS/SS signal $s(n)$, corrupted by the narrowband interference, $j(n)$, and thermal noise $v(n)$. The regularization input is constructed such that it is uncorrelated with $x(n)$. The state vectors are $\mathbf{x}^0_n = [x(n-1)x(n-2)\ldots x(n-N)]^T$ and $\mathbf{r}^0_n = [r(n-1)r(n-2)\ldots r(n-N)]^T$. The regularization is controlled by the scalar parameter β. Refer to Figure 4.1. Rearranging (4.15) and taking expected values yields

$$\mathrm{E}\{\mathbf{w}_{n+1}\} = \mathrm{E}\left\{\left[\mathbf{I} - \mu\left(\mathbf{x}^0_n + \mathbf{r}^0_n\right)\left(\mathbf{x}^0_n - \beta\mathbf{r}^0_n\right)^T\right]\mathbf{w}_n\right\} + \mu\,\mathrm{E}\left\{\left(x(n) - r(n)\right)\left(\mathbf{x}^0_n + \mathbf{r}^0_n\right)\right\} \tag{4.16}$$

Using the standard independence assumptions [41] and that $x(n)$ and $r(n)$ are uncorrelated, (4.16) becomes

$$\mathrm{E}\{\mathbf{w}_{n+1}\} = [\mathbf{I} - \mu\left(\mathbf{R_{xx}} - \beta\mathbf{R_{rr}}\right)]\,\mathrm{E}\{\mathbf{w}_n\} + \mu\left[\mathbf{p}^0_{\mathbf{xx}} - \mathbf{p}^0_{\mathbf{rr}}\right] \tag{4.17}$$

Let $\mathbf{w}^0_{\beta_n} = \mathrm{E}\{\mathbf{w}_n\}$, then substituting into (4.17) and taking the limit as $n \to \infty$ yields [42]

$$\mathbf{w}^0_\beta \triangleq \lim_{n\to\infty}\mathbf{w}^0_{\beta_n} = \mu\left[\mu\left(\mathbf{R_{xx}} - \beta\mathbf{R_{rr}}\right)\right]^{-1}\left[\mathbf{p}^0_{\mathbf{xx}} - \mathbf{p}^0_{\mathbf{rr}}\right] \tag{4.18}$$

Filter Weights	$z(n)-j(n)-v(n)$	$x(n)-j(n)-v(n)$
$\mathbf{w}^0_{WF'}$	$I_{\lfloor n/L \rfloor}c(n)$	$I_{\lfloor n/L \rfloor}c(n)$
$\mathbf{w}^0_{WF_{opt}}$	0	$I_{\lfloor n/L \rfloor}c(n)$
$\mathbf{w}^K_{DF}$	0	0
$\mathbf{w}^0_{\beta}$	$I_{\lfloor n/L \rfloor}c(n) - I'_{\lfloor n/L \rfloor}c'(n)$	$I_{\lfloor n/L \rfloor}c(n) + \beta I'_{\lfloor n/L \rfloor}c'(n)$

Table 4.1.: A summary of the prediction filter inputs and desired responses for the filter designs discussed in the text.

where it is assumed that $\mathbf{w}^0_{\beta_0} = 0$. Convergence is guaranteed if μ is chosen in the range $0 < \mu \leq 1/\max(\lambda(\mathbf{R_{xx}}) + \beta\lambda(\mathbf{R_{rr}}))$, where $\lambda(\mathbf{R_{xx}})$ are the eigenvalues of $\mathbf{R_{xx}}$ and $\lambda(\mathbf{R_{rr}})$ are the eigenvalues of $\mathbf{R_{rr}}$ [42]. Thus, the steady-state weight vector is the solution of

$$[\mathbf{R_{xx}} - \beta\mathbf{R_{rr}}]\,\mathbf{w}^0_{\beta} = \mathbf{p}^0_{x\mathbf{x}} - \mathbf{p}^0_{r\mathbf{r}} \tag{4.19}$$

where regularization is provided by the matrix $\mathbf{R_{rr}}$ and the vector $\mathbf{p}^0_{r\mathbf{r}}$. The scalar β in (4.19) controls the regularization of weight vector solution. The regularization parameter is non-negative, $\beta \geq 0$, with $\beta = 0$ corresponding to the Wiener filter solution.

Expanding terms in (4.19) leads to a form similar to that in (4.14)

$$[\mathbf{R_{jj}} + \mathbf{R_{ss}} + \mathbf{R_{vv}} - \beta\mathbf{R_{rr}}]\,\mathbf{w}^0_{\beta} = \mathbf{p}^0_{j\mathbf{j}} + \mathbf{p}^0_{s\mathbf{s}} - \mathbf{p}^0_{r\mathbf{r}} \tag{4.20}$$

Note that (4.20) is identical in form to (4.14) if $\mathbf{p}^0_{s\mathbf{s}} = \mathbf{p}^0_{r\mathbf{r}}$. This is achieved by constructing the regularization input according to

$$r(n) = I'_{\lfloor n/L \rfloor}c'(n) \tag{4.21}$$

where $I'_{\lfloor n/L \rfloor}$ is independent of $I_{\lfloor n/L \rfloor}$ and is statistically identical to $I_{\lfloor n/L \rfloor}$. The chip sequence $c'(n)$ is statistically identical to the transmitted chip sequence $c(n)$. The cross-correlation between $r(n)$ and $s(n)$ is given by

$$\rho_{rs}(m) = \mathrm{E}\{r(n)s(n+m)\} = \mathrm{E}\left\{I'_{\lfloor n/L \rfloor}\right\}\mathrm{E}\left\{I_{\lfloor n/L \rfloor}\right\}\mathrm{E}\{c'(n)c(n+m)\} \tag{4.22}$$

The cross-correlation function $\rho_{rs}(m) = 0$ due to the zero mean bit sequences. A valid choice for the regularization chip sequence is $c'(n) = c(n+n_0)$, where n_0 is an arbitrary fixed time shift. The autocorrelation function of $r(n)$ is identical to the autocorrelation function of $s(n)$

$$\rho_{rr}(m) = \mathrm{E}\left\{I'_{\lfloor n/L \rfloor}I'_{\lfloor n/L \rfloor}\right\}\mathrm{E}\{c'(n)c'(n+m)\} = \mathrm{E}\left\{I_{\lfloor n/L \rfloor}I_{\lfloor n/L \rfloor}\right\}\mathrm{E}\{c(n)c(n+m)\} \tag{4.23}$$

Using the equivalence $\rho_{rr}(m) = \rho_{ss}(m)$, (4.20) becomes

$$[\mathbf{R_{jj}} + (1-\beta)\,\mathbf{R_{ss}} + \mathbf{R_{vv}}]\,\mathbf{w}^0_{\beta} = \mathbf{p}^0_{j\mathbf{j}} \tag{4.24}$$

Table 4.1 summarizes the associated signals for each filter. It is assumed that the decision-feedback is errorless.

The regularization parameter is chosen to produce minimum SNR degradation from the optimum linear filter in (4.13), which results in

$$\beta = M^2\left(\frac{1+\gamma_c}{\gamma_c}\right)\left(\frac{1}{2L\sigma_j^2 + M^2}\right) \tag{4.25}$$

where γ_c is the SNR per chip, σ_j^2 is the interference power, and $M = \log_2(L+1)$. A few limiting cases of (4.25) are of interest. For vanishing interference power, (4.25) becomes

$$\lim_{\sigma_j^2 \to 0} \beta = \frac{1+\gamma_c}{\gamma_c} \tag{4.26}$$

Note that as the SNR increases in (4.26), β approaches unity. The value $\beta = 1$ effectively removes the excitation to the filter with respect to the mean of the filter weights. For dominant interference power, $\sigma_j^2 \to \infty$, we obtain

$$\beta \sim \left(\frac{1+\gamma_c}{\gamma_c}\right)\left(\frac{M^2}{2L\sigma_j^2}\right) \tag{4.27}$$

If the interference power is large enough, then $\beta \approx 0$. This value for the regularization parameter produces the optimum Wiener filter, that is, $\mathbf{w}^0_{\beta=0} = \mathbf{w}^0_{WF_{opt}}$.

4.4. Performance Results

The regularized interference rejection filter is compared to the optimum Wiener filter with an ideal reference, $\mathbf{w}^0_{WF_{opt}}$ of (4.13), the decision-feedback filter with zero predictive delay, $\mathbf{w}^0_{DF}$ of (4.11) with $K = 0$, the decision-feedback filter with predictive delay equal to the processing gain, $\mathbf{w}^L_{DF}$ of (4.11) with $K = L$, and the optimum Wiener filter which uses the received signal as the reference, $\mathbf{w}^0_{WF'}$ of (4.8). The difference in the filters $\mathbf{w}^0_{WF_{opt}}$ and $\mathbf{w}^0_{WF'}$ is that the former uses exact knowledge of the DS/SS signal $s(n)$, while the latter does not. Thus $\mathbf{w}^0_{WF'}$ is a sub-optimum realizable filter and $\mathbf{w}^0_{WF_{opt}}$ is an optimum unrealizable filter. Similarly, $\mathbf{w}^0_{DF}$ represents an unrealizable filter because it feeds back the signal $s(n)$ before the entire chip sequence is received and the bit can be estimated. The filter $\mathbf{w}^0_{DF}$ will subsequently be termed the symbol-feedback filter because no decision on the bit is involved in the operation of the filter. The filter $\mathbf{w}^L_{DF}$, on the other hand, incurs a delay in the prediction equal to the processing gain L in order to feedback an estimate of the DS/SS signal $s(n)$. In both cases of the feedback filters the exact DS/SS signal is used in the feedback path to avoid error propagation. A filter of length nine taps is used for all filters in the simulations.

The performances of the various filters are simulated by using the discrete time received signal model $x(n) = I_{\lfloor n/L \rfloor} c(n) + j(n) + v(n)$. The narrowband interference, which is uncorrelated with both the DS/SS signal and the random noise, has the form,

$$j(n) = A \sum_{k=0}^{99} \cos\left(\left[\omega_0 + \frac{(k-50)\omega_1}{100}\right] n + \theta_k\right) \tag{4.28}$$

where ω_1 is the spread of the narrowband interference, ω_0 is the frequency deviation from the carrier, θ_k is a random phase uniformly distributed over $(0, 2\pi]$, and A is adjusted to achieve the desired signal-to-interference (SIR) power ratio, which is defined as $\mathrm{SIR} = \mathrm{E}\{s^2(n)\} / \mathrm{E}\{j^2(n)\}$. The input SNR per bit is defined as [31]

$$\gamma_{b_i} = \frac{L}{2\sigma_v^2} \tag{4.29}$$

where σ_v^2 is the variance of the thermal noise. The processing gain used for the simulations is $L = 15$. The SNR per bit at the output of the rejection filter will be calculated

experimentally using [31]

$$\gamma_{b_o} = \frac{\mu_U^2}{\text{var}\,(U)} \tag{4.30}$$

where $\mu_U = (1/K)\sum_{k=1}^{K} U_k$ is the experimental average of the decision variable and $\text{var}(U) = (1/K)\sum_{k=1}^{K} U_k^2 - \mu_U^2$ is the experimental variance of the decision variable. The decision variable is defined as $U_n = \sum_{k=1}^{L} e(\lfloor n/L \rfloor + k)c(k)$ where $e(n)$ is given in (4.2). The number of bits used is $K = 1,000$. The variable ω_0 is taken at ten uniformly spaced intervals over the signal bandwidth and the output SNR is computed at each frequency. These SNR values are subsequently averaged over the ten frequency locations.

Output SNR vs. input SNR

The SIR is set at -6dB with interference bandwidth $\omega_1 = 0.1\pi$, and the output SNR is measured as the input SNR is varied. The results are shown in Figure 4.2. The performance of all the filters is essentially the same below 10dB SNR, except for the decision-feedback filter. It is apparent that there is a large penalty incurred by delaying the symbol feedback by an amount equal to the processing gain. The regularized filter performance is slightly (1dB) better than the optimum Wiener filter using the ideal reference for all input SNR. The regularized filter is 1.5dB better at 20dB SNR than the optimum realizable Wiener filter that uses the received signal as a reference. As expected, the symbol-feedback filter performs the best and is 1dB better than the regularized filter at 20dB SNR. The separation of the filter performance curves as the SNR increases is a manifestation of the effects of the filter self-noise.

Output SNR vs. input SIR

For this simulation, the input SNR is fixed at 20dB with normalized interference bandwidth $\omega_1 = 0.1\pi$ and the output SNR is measured as the SIR is varied. The results are shown in Figure 4.3. As the interference power decreases, the regularized filter SNR approaches the symbol-feedback filter SNR as can be expected. The regularized filter SNR exceeds the optimum realizable Wiener filter SNR by approximately 2dB, when the SIR exceeds 0dB. There is again a substantial penalty for delayed decision feedback in the region of SIR below 0dB. However, the output SNR for this filter improves dramatically when the SIR exceeds 0dB.

4.5. Summary

A regularized LMS interference rejection filter is developed, which is based upon reducing the self-noise of the filter. The regularized LMS filter is obtained by using a weighted sum of the received signal with a regularization signal as the input to the normal adaptive LMS update algorithm. The regularization input shares the same autocorrelation function as the transmitted DS/SS signal, which allows a trade-off of interference rejection and filter self-noise reduction. performance results are presented that show the performance improvement afforded by the regularized LMS filter. The regularized interference rejection filter was compared to the optimum Wiener filter and the decision-feedback filter. The increase in output SNR compared to the Wiener filter was 1.5dB for SIR=-6dB. The increase in output SNR for moderate to high SIR was 2.5dB. The regularized filter also achieved the performance of the optimal decision-feedback filter for SIR exceeding 0dB. The optimum Wiener filter is the one obtained when using only the interference as the reference signal for the adaptive filter. The optimal decision-feedback filter subtracts the correct symbol from the filter input without delay. The practical decision-feedback filter is the one that subtracts the correct symbol only after it is correctly estimated at the correlator output.

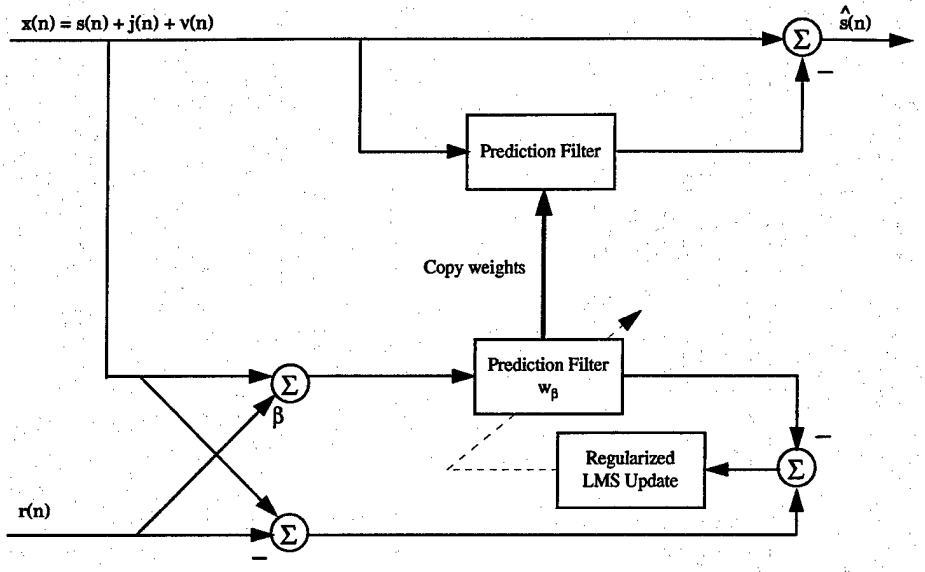

Figure 4.1.: The rejection filter update uses the LMS algorithm and is regularized by the input $r(n)$. The regularization is controlled by β.

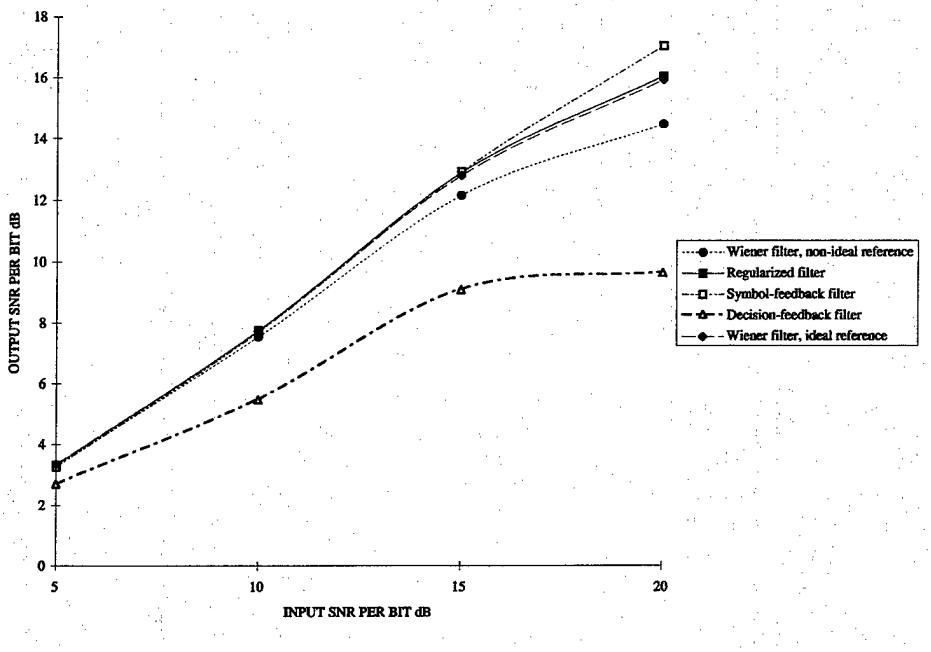

Figure 4.2.: Output SNR vs. input SNR. SIR=6 dB, processing gain=15, prediction filter length= 9, interference bandwidth $\omega_1 = 0.1\pi$.

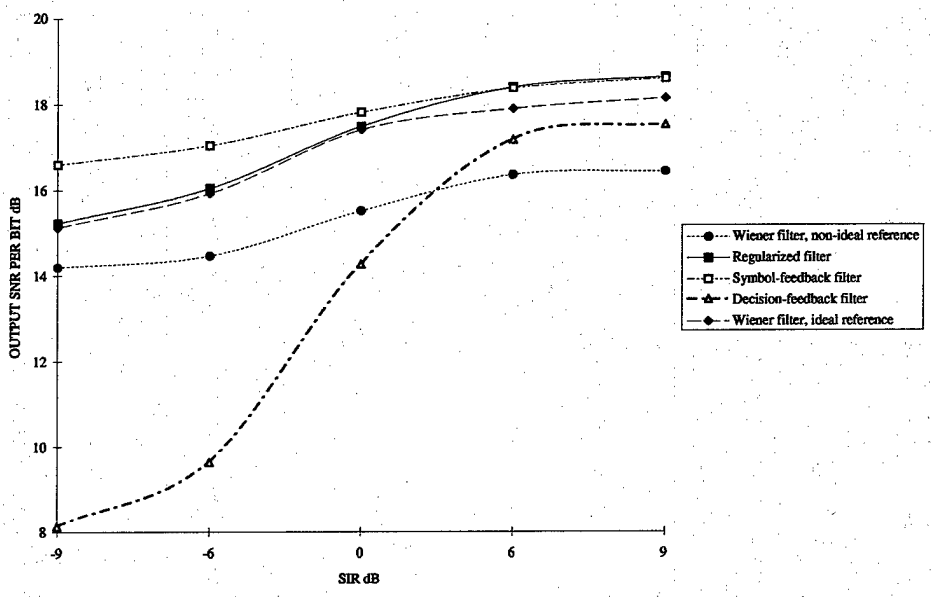

Figure 4.3.: Output SNR vs. input SIR. SNR=20dB, processing gain=15, prediction filter length=9, interference bandwidth $\omega_1 = 0.1\pi$.

5. IS-95 CDMA System Modeling

A system level simulation model for the IS-95 Code Division Multiple Access Spread Spectrum communication link is developed. The simulation is carried out in SIMULINK®, a dynamic system simulation toolbox in MATLAB®, that provides a graphical framework closely integrated with implementation tools. The building blocks used at the top-level consist of models of an information source, baseband processing, QPSK modulator, multipath fading channel, RAKE demodulator and decoder. Link metrics such as bit error rate (BER) and signal-to-noise ratio (SNR) that are directly dependent on transmitter and receiver implementations as well as radio channel characteristics and provide an objective measure of performance are evaluated.

5.1. Introduction

Prospective proliferation of mobile radio communication systems calls for increased capacity, reduced cost, improved performance, and dual-mode operational requirements. The IS-95 *Mobile-Station Base-Station Compatibility Standard For Dual-Mode Wideband Spread Spectrum Cellular System* is endorsed by the US Telecommunications Industry Association / Electronic Industry Association (TIA/EIA). It is based on code division multiple access (CDMA) technique that conforms to these specifications [52]. CDMA direct sequence spread spectrum technique (DSSS), incorporated into this system, enables the accommodation of a large number of users in one radio channel depending on the voice activity level [53], i.e., it is interference limited unlike frequency and time domain multiple access based systems that are bandwidth limited. This feature also provides immunity to jamming signals and enables resolution of multipath components in a time-dispersive radio propagation channel [51].

Accurate prediction of the performance of such systems has become increasingly important. Simulation technology that can be integrated into implementation tools has provided researchers and designers an efficient solution to this problem. Moreover, manufacturers greatly rely on communication system simulations to develop specific implementations before hardware development to reduce cost and to improve flexibility. Analytical techniques, by comparison, are intractable when representing complex communication systems operating in time-varying radio channels. Current generation workstation based simulation software packages provide interactive, hierarchical and graphical framework for link-level and system wide simulations, e.g. BOSS®, SPW® and COSSAP® [48]. SIMULINK® is another dynamic system simulation software based on MATLAB® that is widely available and provides a real-time simulation platform in addition to features listed above. Moreover, MATLAB® provides the necessary implementation tools to download the simulated system models into programmable digital signal processors

The communication system model is typically a block diagram description of various interconnected subsystems comprising the overall system. Link-level simulations focus on performance measures such as signal-to-noise ratio (SNR) and bit error rate (BER) of a communication link. Such link metrics are affected by multipath fading conditions within the channel and receiver implementations. Efficient simulation of the signal processing operations modeling the system then becomes critical in the evalu-

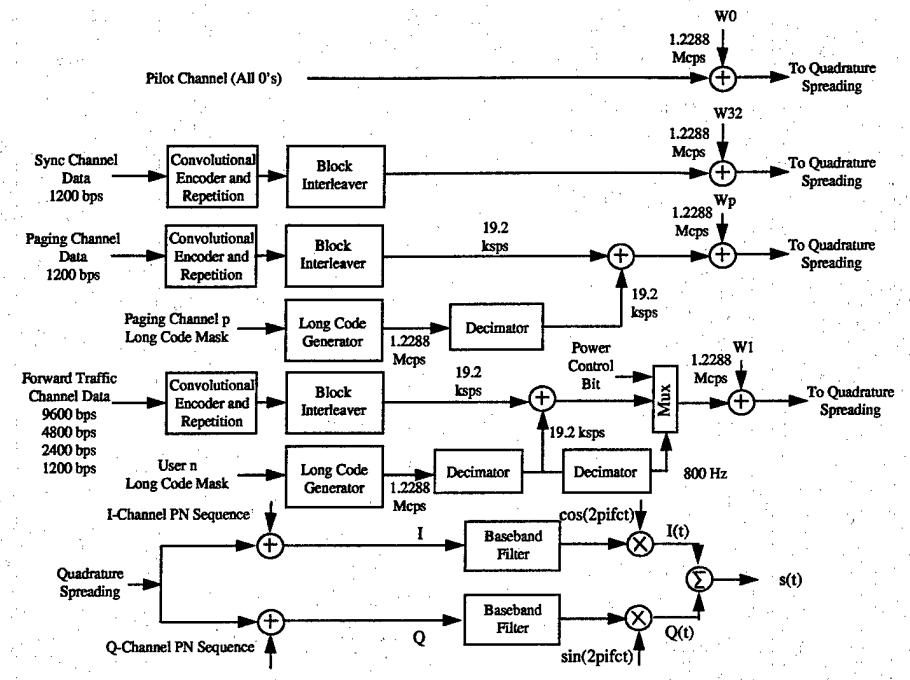

Figure 5.1.: Forward CDMA Channel Structure.

ation of its performance. Also, the entire system including the environment in which it operates must be simulated. This can be done using analytical models, statistical models based on experimental observations, experimentally measured channel impulse responses or from the geometry of the environment. Since only the second and third methods are feasible, channel impulse responses (also estimated as power delay profiles from field trial measurements) were used to model the multipath fading environment.

5.2. System Description

The IS-95 standard proposes a system consisting of forward (base station to mobile station) and reverse (mobile station to base station) CDMA channel structures, which are described in the following sections.

Forward CDMA Channel Structure

The forward CDMA channel consists of four code channels : the pilot channel (always required), the sync channel, paging channels (1 to 7) and traffic channels (55 to 63)(see Figure 5.1) [52]. Pilot channel, transmitted at all times, is an unmodulated spread spectrum signal used for synchronization by a mobile station operating within the coverage area of the base station. The sync channel is a modulated spread spectrum signal used by mobile stations to acquire initial time synchronization. The paging channel is also a modulated spread spectrum signal used to transmit system overhead information by the base station and specific messages by the mobile station. The forward traffic channel is used for the transmission of user and signaling information to a specific mobile station during a call.

Data rates at the input are : Pilot channel (all 0's) at 19.2 kbps; Sync channel at 1.2 kbps; Paging channel (fixed data rate) at 9.6, 4.8 or 2.4 kbps; Traffic channel (variable data rate) at 9.6, 4.8, 2.4 or 1.2 kbps. The sync, paging and traffic channel data are

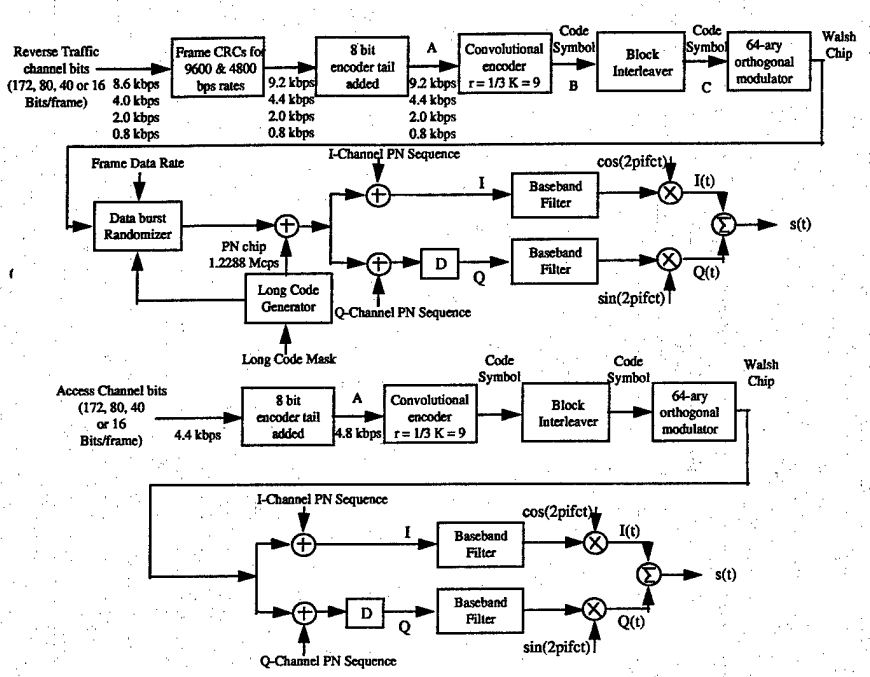

Figure 5.2.: Reverse CDMA Channel Structure.

then convolutionally encoded using rate 1/2, constraint length 9 code. A long-code (of length 2^{42}-1) at the PN chip rate (1.2288 Mcps or million chips per second) spreads the encoded symbols. A long code mask that modulates the long code in traffic channels is used for voice privacy.

Each code channel transmitted on the forward CDMA channel is spread with a Walsh function at a fixed chip rate of 1.2288 Mcps to provide orthogonal channelization among all code channels. After orthogonal spreading, each of these code channels are spread by a quadrature pair of maximal-length PN sequences (length 2^{15}) at a fixed chip rate of 1.2288 Mcps. PN sequence time offsets are used in code channels for synchronization by a mobile station. The base station transmits the forward CDMA channel signal at 870.030 MHz with a channel spacing of 30 kHz. The corresponding dual-mode mobile station transmit channel is at 825.030 MHz.

Reverse CDMA Channel Structure

The reverse CDMA channel is composed of access channels and reverse traffic channels. The reverse channel is 64-ary orthogonal modulated at data rates of 9.6, 4.8, 2.4 or 1.2 kbps as shown in Figure 5.2 at point A. The rate of the spreading PN sequence is fixed at 1.2288 Mcps. The reverse traffic channel is used for the transmission of user and signaling information to the base station during a call. The access channel is used by the mobile station to initiate communication with the base station and to respond to

paging channel messages. The mobile station transmits information on the reverse traffic channel at variable data rates of 9.6, 4.8, 2.4 or 1.2 kbps and on the access channel at a fixed data rate of 4.8 kbps. These are then convolutionally encoded by rate 1/3, constraint length 9 codes. The code symbols are then modulated by a 64-ary orthogonal modulator using 64 Walsh functions. The reverse traffic channel and the access channel are then direct sequence spread by the long code. Furthermore, the

waveform is spread by a pair of PN codes (identical to the ones used in the forward traffic channel), common to all subscribers and to the access channel in an OQPSK arrangement. The final waveform is then filtered to generate a spectrum with 1.2288 MHz double-sided 3 dB bandwidth. The mobile station transmits the reverse CDMA channel signal at 825.030 MHz with a channel spacing of 30 kHz. The corresponding dual-mode base station transmit channel is at 870.030 MHz.

Receiver

The mobile station demodulation process involves complementary operations to the base station modulation process. The mobile station also performs tracking and demodulation of multipath components of the forward CDMA channel in addition to scanning and estimation of the signal strength at each pilot PN sequence offset. The standard specifies the use of a RAKE correlator in the receiver but its structure is not specified.

5.3. System Modeling and Simulation

A communication system based on the IS-95 standard is developed from a software-representable description or a block diagram of the system described in the previous section. Each block represents a subsystem that can be described using signal-processing operations. An explicit model vis-a-vis, the equations and algorithms or methodologies followed in the implementation of each operation is presented here.

Random Data Generator

Forward and reverse traffic channel information bits are simulated as digital signals containing embedded digital sequences represented as

$$X(t) = \sum_{k=-\infty}^{\infty} A_k p(t - kT_b - D) \tag{5.1}$$

where $\{A_k\}$ is a digital sequence, T_b is the bit period, D is a random delay and p(t) is a suitable pulse waveform.

A general block to implement (5.1) is developed using the random number generator in SIMULINK [49]. The pulse waveform and delay are incorporated into this block as shown in Figure 5.3.

The user interface to this subsystem has controls for specifying the time period or the data rate, random delay and the seed for the random number generator. Different seeds are used to distinguish between the code channels and initial delays are set to zero for link-level simulations.

Convolutional Encoder

A linear binary shift register made up of unit delay blocks in SIMULINK is used to implement convolutional encoders. The code characteristics are established by feedback taps which are defined by generator functions.

The forward channel at the base station uses a convolutional code of rate 1/2 and constraint length 9. The generator functions of the code are 753 (octal) for g_o and 561 (octal) for g_1. Two code symbols are generated for each data bit. These code symbols are output such that code symbol (c_o) encoded with generator function g_o is output first and code symbol (c_1) encoded with generator function g_1 is output last (see Figure 5.4).

The modulo-2 adders are implemented using XOR gates and the outputs of g_o and g_1 multiplexed to form the output sequence of code symbols at twice the input data rate.

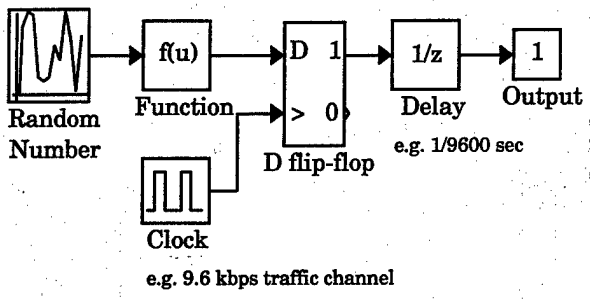

Function = ceil(u[1]) && floor(u[1])
where u[1] is the input.

Figure 5.3.: Random Data Generator.

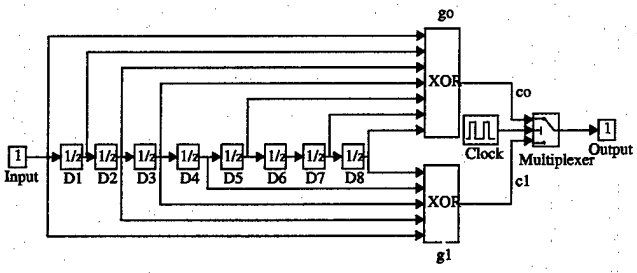

D : Unit delay block used as a shift register.
XOR gates are used for Modulo-2 Adders
c_0 : 753 (octal); c_1 : 561 (octal)

E.g. Input data rate = 9600 kbps for traffic channel
Clock = 19200 KHz

Figure 5.4.: Convolutional Encoder, K = 9, Rate = 1/2.

The reverse channel uses a convolutional code of rate 1/3 and constraint length 9 with generator functions g_o equal to 557(octal), g_1 equal to 663(octal) and g_2 equal to 711(octal). Three code symbols are generated for each data bit and are output such that code symbol c_o encoded with generator g_o is output first, c_1 second and c_2 last. This is implemented as described for the forward channel.

Walsh Code Generator

Each code channel transmitted on either CDMA channel is spread with a Walsh function to provide orthogonal channelization among all code channels. One of sixty-four time-orthogonal Walsh functions is used for the purpose. The 64 x 64 matrix of Walsh functions is generated using the following recursive procedure:

$$H_1 = 0 \qquad H_2 = \begin{bmatrix} 0 & 0 \\ 0 & 1 \end{bmatrix}$$
$$H_4 = \begin{bmatrix} 0 & 0 & 0 & 0 \\ 0 & 1 & 0 & 1 \\ 0 & 0 & 1 & 1 \\ 0 & 1 & 1 & 0 \end{bmatrix} \quad H_{2N} = \begin{bmatrix} H_N & H_N \\ H_N & \overline{H_N} \end{bmatrix} \tag{5.2}$$

where N is a power of 2 and $\overline{H_N}$ denotes the binary complement of H_N.

The repeating sequence block in SIMULINK calls the MATLAB file that uses the built-in function *hadamard.m.* A 64 x 64 Hadamard matrix is first generated using the recursive procedure described above. The elements of the Walsh function are then obtained by mapping the binary alphabet of {-1,1} of the Hadamard matrix into the binary alphabet of {1,0} of the Walsh function matrix. Input to this block is the Walsh function number and output is the corresponding Walsh function.

Long Code Generator

Forward and reverse traffic channel data are direct sequence spread by a long code of length 2^{42} -1 chips. The long code satisfies the linear recursion specified by the characteristic polynomial given by

$$\begin{aligned} p(x) \quad = \quad & x^{42} + x^{35} + x^{33} + x^{31} + x^{27} + x^{26} + x^{25} + x^{22} + x^{21} + x^{19} + x^{18} + \\ & x^{17} + x^{16} + x^{10} + x^7 + x^6 + x^5 + x^3 + x^2 + x + 1 \end{aligned} \tag{5.3}$$

The code is generated by the modulo-2 inner product of a 42-bit mask and the 42-bit state vector of the sequence generator using AND gates. Mobile identification number is incorporated into the 42-bit mask for voice privacy. A 42-bit random repeating sequence is used for simulation purposes.

PN Sequence Generators

Following orthogonal spreading, each code channel is spread in quadrature. The spreading sequence is of length 2^{15}. The maximum length linear feedback shift register sequences i(n) and q(n) are based on the polynomials of length 2^{15} -1 given by

$$P_I(x) = x^{15} + x^{13} + x^9 + x^8 + x^7 + x^5 + 1 \tag{5.4}$$

$$P_Q(x) = x^{15} + x^{12} + x^{11} + \ x^{10} + x^6 + x^5 + x^4 + x^3 + 1 \tag{5.5}$$

The I and Q pilot PN sequences are obtained by inserting a '0' in i(n) and q(n) after 14 consecutive '0' inputs (this occurs once in each period). This is achieved using a repeating sequence block that inserts a zero appropriately.

QPSK Modulator

Baseband filters used for filtered QPSK modulation are derived from the filter coefficients specified in the standard and are implemented using the Discrete Filter block in

Table 5.1.: I and Q Mapping

I	Q	Phase
0	0	$\pi/4$
1	0	$3\pi/4$
1	1	$-3\pi/4$
0	1	$-\pi/4$

SIMULINK. The filtered and quadrature spread I and Q channel sequences phase-shift modulate in-phase and quadrature phase carriers in a pseudo-random fashion resulting in direct sequence spread spectrum modulation. I and Q channel phase mapping is given in Table 5.1. The output signal can be expressed as

$$S(t) = I(t)\cos(2\pi f_c t) - Q(t)\sin(2\pi f_c t) \tag{5.6}$$

where I(t) and Q(t) are the filtered waveforms with embedded I and Q channel digital sequences respectively represented as

$$\begin{aligned} I(t) &= \sum_{k=-\infty}^{\infty} Ip(t - kT_c) \\ Q(t) &= \sum_{k=-\infty}^{\infty} Qp(t - kT_c). \end{aligned} \tag{5.7}$$

f_c is the transmit frequency (870.030 MHz) and T_c is one chip period (813.802 ns).

For OQPSK modulation on reverse channel, the Q channel data is offset such that

$$Q(t) = \sum_{k=-\infty}^{\infty} Qp(t - kT_c - T) \tag{5.8}$$

where T is half a chip period (409.901 ns). S(t) can also be expressed as

$$S(t) = \mathrm{Re}\{\tilde{S}(t)e^{j2\pi f_c t}\} \tag{5.9}$$

where $\tilde{S}(t)$ is the complex envelope or the low-pass equivalent representation given by

$$\tilde{S}(t) = [I(t) + jQ(t)]. \tag{5.10}$$

RF carriers required for the modulation process are implemented using the sine blocks in SIMULINK with frequency f_c, phase 0 and $\pi/2$ and unit amplitudes. Product and difference operations are implemented using suitable blocks from the SIMULINK library (see Figure 5.5).

5.4. Multipath Channel Model

Channel simulation requires accurate representation of the signal environment for the desired frequency and geographic location. Experimentally measured channel impulse responses, also known as power delay profiles, are used for channel modeling. Wireless transmissions undergo multipath-induced fading as the radiated energy interacts with objects within the channel. Under these conditions, link-level simulations require the simulation of small scale fading effects, impulsive noise and short term variations of multipath channel impulse responses to determine realistic bit error patterns. The

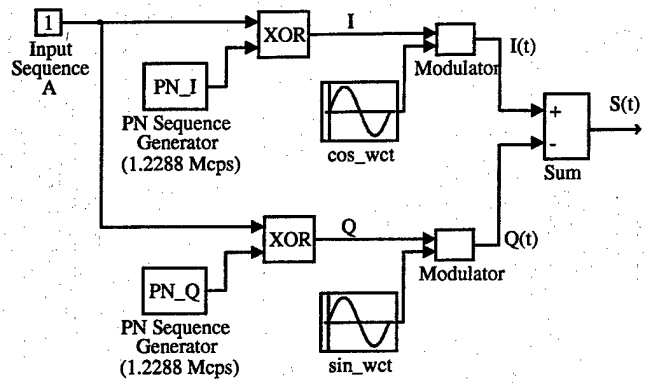

Figure 5.5.: Forward CDMA Channel QPSK Modulator.

fading signal has known to have three basic components contributing to the variations in its signal strength described as follows.

Propagation Path Loss

The free space propagation path loss is due to the frequency of transmission and the distance of the mobile from the base station and can be described as,

$$\frac{P_{or}}{P_t} = \left[\frac{1}{4\pi d(f/c)}\right]^2 = \left[\frac{1}{4\pi(d/\lambda)}\right]^2 \tag{5.11}$$

where c is the speed of light, λ is the wavelength, P_t is the transmitted power and P_{or} is the received power in free space. Gain blocks of SIMULINK were used to incorporate this in the simulated multipath channel model.

Long-Term Fading

Long-term fading or slow fading is caused by movement of the mobile over distances large enough to produce gross variations in the overall path between the transmitter and receiver. This results in attenuation and fluctuations in the local-mean of the fading signal. Measurements indicate that the mean path loss closely fits a log-normal distribution with a standard deviation that depends on the frequency and environment [51]. Standard deviations of 8 dB and 6 dB were used for suburban and urban environment models. The lognormal pdf can be represented as

$$p(y) = \frac{1}{\sqrt{2\pi}\sigma_y} \exp\left[-\frac{(y-m)^2}{2\sigma_y^2}\right] \tag{5.12}$$

where the lognormal variable y, its mean m, and its standard deviation σ_y are in dB scales [50]. Lognormal variations in the local mean of the signal were brought about using the random number generator and the logarithm function blocks as in Figure 5.3.

Short-Term Fading

Short-term fading is caused by multipath reflections of a transmitted wave by local scatterers such as buildings and forests surrounding a mobile unit. Many researchers have shown that the envelope of the mobile radio signal is Rayleigh distributed. This suggests that at any point, the received field is made up of a number of horizontally

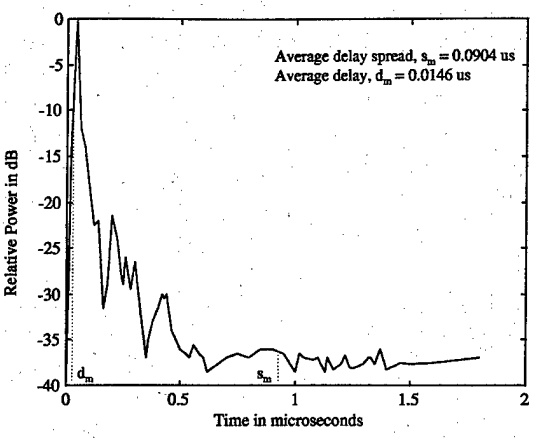

Figure 5.6.: Sample Power Delay Profile.

traveling plane waves with random amplitudes and angles of arrival for different locations. The phases of the waves are uniformly distributed from 0 to 2π. The amplitudes and phases are assumed to be statistically independent.

The Rayleigh pdf is represented as

$$p(r) = \frac{r}{\sigma^2} \exp\left(-\frac{r^2}{2\sigma^2}\right) \tag{5.13}$$

where σ^2 is the average power of the short-term fading signal.

Simulated Multipath Channel Model

Experimental evidences such as those described above gave rise to a three-stage model to describe mobile radio propagation, an inverse n-th power law with range from the transmitter to the receiver, lognormal variations of the local mean and superimposed fast fading which follows a Rayleigh distribution. Since Rayleigh fading is caused by the combined effect of time delayed components of the radio signal reaching the receiver, a discrete model based on the channel impulse response was developed.

A typical power delay profile is shown in Figure 5.6 and is given by

$$P_m(\tau_k) = \frac{1}{M} \sum_{i=1}^{M} p_i(\tau_k). \tag{5.14}$$

A measure of the width of an average power delay profile that is relevant in assessing the impact on a communications system performance is delay spread, s_m, defined as the square root of the second central moment of a profile m and expressed as

$$s_m \triangleq \left[\frac{\sum_{k=1}^{K}(\tau_k - d_m - \tau_A)^2 P_m(\tau_k)}{\sum_{k=1}^{K} P_m(\tau_k)}\right]^{1/2} \tag{5.15}$$

where k ranges over the entire time duration of the measuring window, τ_k is the time delay of the kth sample and d_m is the average delay, the first moment of the profile with respect to the first arrival delay τ_A, defined as

$$d_m \triangleq \frac{\sum_{k=1}^{K} \tau_k P_m(\tau_k)}{\sum_{k=1}^{K} P_m(\tau_k)} - \tau_A. \tag{5.16}$$

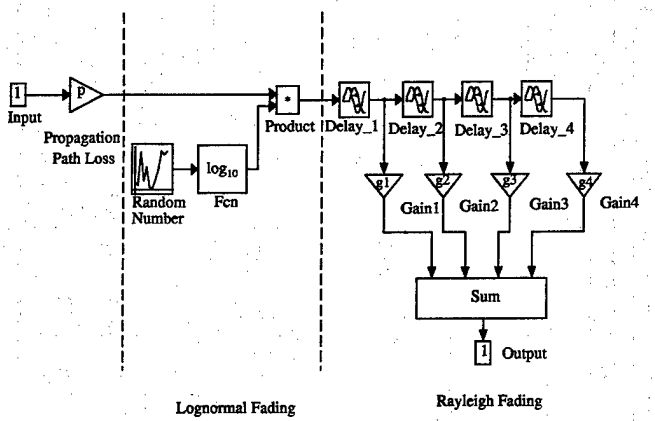

Figure 5.7.: Multipath Channel Model.

The delay of the last significant component above -10 dB in the power delay profile is called the average excess delay, E_d. The energy of the signal outside the window between τ_A and E_d is negligible and is set to zero for computations of the tap gains and tap delays in the RAKE receiver.

Measurements of power delay profiles from [1,2,7,9,11] are incorporated into the discrete model for the multipath channel (see Figure 5.7). This provided measurement based channel models for performance evaluation of the communication system. Values of parameters α_n, the attenuation along the path arriving after a time delay, τ_n were estimated from the power delay profiles and used in the gain and transport delay blocks of the simulated multipath channel model.

5.5. Receiver Structure

The standard specifies a receiver that performs demodulation process comprising of complementary operations to the transmitter modulation process. QPSK and OQPSK demodulation are carried out using local carrier references. In the actual case, pilot and sync channels are used for carrier recovery and symbol and frame synchronization respectively. For simulation purposes, perfect carrier recovery and time synchronization are assumed. From the received signal r(t) = S(t)+n(t), (n(t) is additive white Gaussian noise, N(0,σ^2)) the demodulated outputs $I_o(t)$ and $Q_o(t)$ are obtained as follows:

$$\begin{aligned}
I_o(t) &= \tfrac{2}{T_c}\int_0^{T_c} r(t)\cos(2\pi f_c t+\theta)dt \\
&= \tfrac{1}{T_c}\int_0^{T_c}\left[2I(t)\cos^2(2\pi f_c t+\theta)-2Q(t)\sin(2\pi f_c t+\theta)\cos(2\pi f_c t+\theta)\right]dt \\
&= \tfrac{1}{T_c}\int_0^{T_c}\left[I(t)\left\{1+\cos[2(2\pi f_c t+\theta)]\right\}-Q(t)\sin[2(2\pi f_c t+\theta)]\right]dt \\
&\simeq I(t) \\
Q_o(t) &= \tfrac{2}{T_c}\int_0^{T_c} r(t)\sin(2\pi f_c t+\theta)dt \\
&= \tfrac{1}{T_c}\int_0^{T_c}\left[-2I(t)\cos(2\pi f_c t+\theta)\sin(2\pi f_c t+\theta)+2Q(t)\sin^2(2\pi f_c t+\theta)\right]dt \\
&= \tfrac{1}{T_c}\int_0^{T_c}\left[-I(t)\sin[2(2\pi f_c t+\theta)]+Q(t)\left\{1-\cos[2(2\pi f_c t+\theta)]\right\}\right]dt \\
&\simeq Q(t)
\end{aligned} \tag{5.17}$$

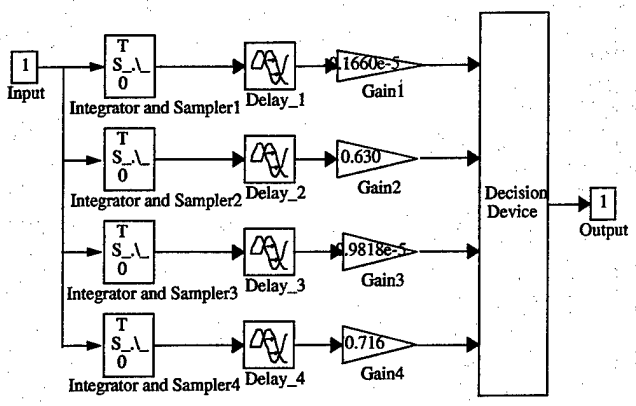

Figure 5.8.: RAKE Receiver Structure.

The local references are implemented using the sine blocks in SIMULINK. The integrator and sampler block performs integration of the input waveform over one chip period and outputs this value at the end of the chip period. The integrator is reset after every chip period, T_c (=813.802 ns). This is implemented using the integrator, sample and hold blocks in SIMULINK.

RAKE Correlator

A RAKE correlator is used to overcome multipath fading effects of the diversity communications system. It is a tapped delay line receiver that attempts to collect the signal energy from all the received signal paths that fall within the span of the delay line and carry the same information. Hence it is an optimum receiver for processing wideband signals that suffer from multipath fading effects.

The structure of the RAKE correlator is not specified in the standard. Path loss characteristics of measurements in [1,2,7,9,11] were used to estimate the number of taps and tap gains in the correlator shown in Figure 5.8. The RAKE receiver is then implemented using the transport delay blocks for the delays and gain blocks for the tap gains in SIMULINK.

The taps on the RAKE receiver are synchronized to the detected paths in the received signal using the delay blocks. The decision variable is obtained from the noncoherent combination of the matched filter (integrator and sampler) outputs. This is achieved by delaying these outputs and synchronizing them at a time equal to $(T + \Delta w)$ where T is the estimated time from the symbol synchronization and Δw is the maximum delay of the radio channel. If the correlator outputs are represented as $\xi(T - \tau_i)$, $i = 1, 2..K$ where τ_i is the ith time delay and K is the number of paths, the decision variable can be expressed as

$$\varsigma = \sum_{i=1}^{K} \beta_i \xi_i (T + \Delta w) \tag{5.18}$$

where β_i is the normalized tap gain corresponding to the strength of the ith path. The decision block outputs a '1' for $\varsigma < 0$ and '0' for $\varsigma \geq 0$. Such a RAKE receiver is called noncoherent or optimum combining RAKE receiver.

5.6. Performance Results

Simulations for the complex communication system developed here rely on a quasi-static approach where the channel is static for a specific period of time when specific conditional performance measures such as signal-to-noise ratio (SNR) and the accumulated signal distortions in terms of the bit error rate (BER) are estimated. The simulated data and code generators are tested for statistical and correlation properties to verify their functionality. The convolutional encoders are tested in terms of its impulse response by observing its output for a single '1' bit input. The orthogonality property of the implemented Walsh codes or functions are tested.

BER Estimation

Monte Carlo is the name for implementation of a sequence of Bernoulli trials where the number of 'successes' (errors) are divided by the number of trials. For link-level simulations considered here, this technique lends itself well to performance evaluation of RAKE correlators used to compensate for multipath fading effects. The source output (known) is compared with a delayed version of the decision device output to obtain an empirical basis for the error rate.

Importance sampling is a form of Monte Carlo simulation in which the statistical properties of the noise processes driving the system are altered such that many more errors are produced per unit time. A known change is introduced and is corrected for enabling a reduction in simulation run time Since the system under consideration has various noise sources with varying distributions (lognormal, Rayleigh and Rician) causing alteration and correction of their parameters to be computationally intensive, this simulation methodology was not adopted.

SNR Estimation

The standard measure of performance for a noisy signal is the signal-to-noise ratio (SNR). Assuming that output of the decision block after the RAKE receiver is a signal corrupted by additive noise, the SNR estimate $\hat{\rho}$ is given by

$$\hat{\rho} = \langle s_0^2 \rangle / \varepsilon^2 \tag{5.19}$$

In the system under consideration, s_0 is a pulse waveform with amplitude, $A = 1$ and ε^2 is the time average of the square of difference in the source and output digital waveforms.

Receiver Characteristics

The performance characteristics of the communication system in multipath cellular environment is of interest here. Hence the 2^{15} long PN sequence was QPSK modulated with a carrier frequency of 870 MHz, passed through the multipath channel and detected using a RAKE demodulator. The BER and SNR were estimated and the performance characteristics of the system determined.

A four-way RAKE receiver to demodulate the four strongest multipath components received on two diversity antennae was used during prototype validation. In this configuration, the decision output from each of the active demodulators is fed to an external microprocessor. The microprocessor combines the individual demodulator decisions, weighing each one by the relative strength of the respective multipath component and generates a single stream of soft-decision inputs to the Viterbi decoder. But this type of diversity combining is sub-optimal since an independent decision on the transmitted orthogonal symbol is being made by each individual demodulator.

Hence an optimum combining diversity receiver was developed where the number of taps are equal to the number of paths in the power delay profile and the tap gains were estimated from the strength of the signal component along the corresponding path. The test setup is shown in Figure 5.9.

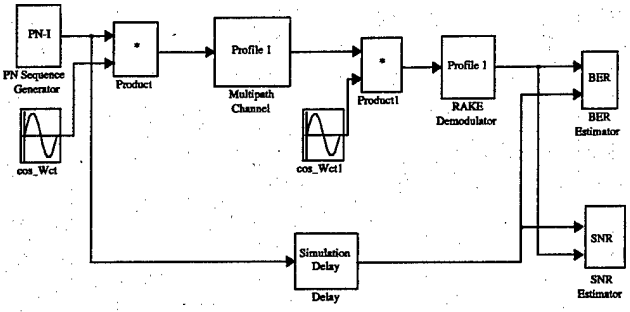

Figure 5.9.: Performance Test Setup.

Table 5.2.: Observed Channel Characteristics

Type of Channel	Number of Paths, K	Average Delay Spread, s_m (in μs)
Open Area	$K < 4$	$0.5 < s_m < 0.9$
Suburban	$5 < K < 8$	$1 < s_m < 5$
Urban	$8 < K < 15$	$s_m \geq 3$
Indoor	$K > 5$	$s_m < 1$

The noise threshold chosen to distinguish between a signal and noise component was -94 dBm [48]. Profile 1 is the file containing power delay profile measurements obtained from [53] for a suburban environment. The obtained performance characteristics are shown in Figure 5.10. Optimum combining RAKE receiver shows a 2.5 dB improvement in the required SNR for a BER of 10^{-3}.

Multipath Channel Characteristics

Time-delayed echoes in multipath channels can overlap causing errors in digital systems due to inter symbol interference. In this case, increasing the signal-to-noise ratio will not cause a reduction in error rate and so the delay spread sets the lower bound on error performance for a specified data rate. This limit is often termed as the irreducible error rate. The performance of the system can however be improved by the use of channel equalization and diversity (RAKE receiver) techniques.

Some of the observed characteristics in the power delay profiles of open area, suburban, urban and indoor environments are tabulated in Table 5.2. A noise threshold of -94 dBm or 35 dB below the strongest component was used to distinguish between signal and noise components and to estimate the number of paths and the average (or rms) delay spreads from the power delay profile measurements.

Open area environments are characterized by very small average delay spread values with less than 4 paths. The direct component is almost always present in them and they do not require channel equalization. Suburban environments also provide a good propagation medium when the direct component is present and the reflected components are well above the noise floor. Hence diversity combining proves highly efficient for such environments. Urban and indoor channels, however, have many reflected paths and can be differentiated by the fact that the latter have shorter paths

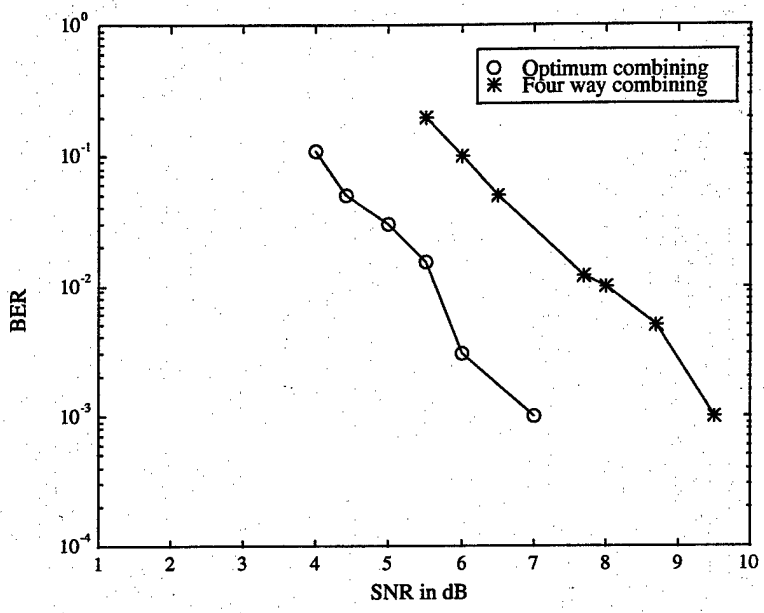

Figure 5.10.: Comparison of BER Vs SNR for optimum and four-way combining RAKE diversity receiver.

and hence considerably smaller average delay spread values.

5.7. Summary

A software simulation technique to implement an IS-95 standard based CDMA spread spectrum communication system in SIMULINK is developed. Major subsystems (encoders, modulators, demodulators) required to estimate the performance of the system in a mobile cellular environment are simulated and tested. A multipath channel model consisting of lognormal and Rayleigh fading simulators and a path loss component is implemented. The simulated system thus enables subjective quality evaluation of mobile radio links. The performance of the system with regard to BER is determined and compared for 4-way and optimum combining RAKE receivers. The optimum combining RAKE receiver provides 2.5 dB improvement in SNR for a BER of 10^{-3}.

Characteristics of multipath channels for open area, suburban, urban and indoor environments with regard to average delay spread and number of discrete paths are compared based on power delay profile measurements. The delay spreads by themselves do not provide very precise measures for system evaluation. It is therefore more useful to provide statistics about the number of paths and their time delays. These results can then be used in designing hardware and software simulators such as diversity combining receivers.

6. Publications

- J. Yoon and J. F. Doherty, "Adaptive Interference Suppression in CDMA Systems with Large Processing Gains," *Proceedings of the IEEE Military Communications Conference*, Boston, MA, Oct. 1998.
- Y. Hsieh and J. F. Doherty, "Block Iterative Algorithm for Multiple-Access Interference Suppression," submitted to *IEEE Communications Letters*, Sep. 1998.
- J. Yoon and J. F. Doherty, "Interference Suppression in CDMA Systems Using a Decomposed Adaptive Receiver," submitted to *IEEE Communications Letters*, Sep. 1998.
- Y. Hsieh, "Block Iterative Algorithm For Multiple-Access Interference Suppression," M.S. Paper, The Pennsylvania State University, University Park, PA, August 1998.
- J. Koo, "CDMA Receiver using Zero-Crossing Algorithm," M.S. Paper, The Pennsylvania State University, University Park, PA, August 1998.
- J. F. Doherty, "A Regularized LMS Algorithm for Interference Rejection in Direct Sequence Spread Spectrum Communications," *Wireless Personal Communications: An International Journal*, Kluwer Academic Publishers, vol. 7, issue 1, pp. 53-67, May 1998.
- S. C. Park and J. F. Doherty, "Generalized Projection Algorithm for Blind Interference Suppression in DS/CDMA Communications," *IEEE Transactions on Circuits and Systems II: Analog and Digital Signal Processing*, **Special Issue on Low-Power Wireless Communication**, vol. 44, no. 6, pp. 453-460, June 1997.
- S. C. Park, "Blind Adaptive Near-Far Resistant Receivers for DS/CDMA Multiuser Communication Systems," Ph.D. Thesis, Iowa State University, Ames, IA, December 1996.
- V. Raveendran, "Performance Characteristics of the IS-95 Standard for CDMA Spread Spectrum Mobile Communications Systems," M.S. Thesis, Iowa State University, Ames, IA, December 1996.
- S. C. Park and J. F. Doherty, "A Constrained Adaptive Algorithm for Multiple-Access Interference Suppression," *Proceedings of the IEEE Military Communications Conference*, McLean, VA, Oct. 1996.
- V. R. Raveendran and J. F. Doherty, "Optimum Combining RAKE Receivers for DS/CDMA Mobile Communication Systems," *Proceedings of the Seventh International Conference on Signal Processing Applications and Technology*, Boston, MA, Oct. 1996.
- V. R. Raveendran and J. F. Doherty, "Performance Characteristics of the IS-95 Standard for CDMA Communications Systems," *Proceedings of the IEEE Midwest Symposium on Circuits and Systems*, Ames, IA, Aug. 1996.

• S. C. Park and J. F. Doherty, "A Robust Self-Adaptive Method for Multiple-Access Interference Suppression," *Proceedings of the IEEE Midwest Symposium on Circuits and Systems*, Ames, IA, Aug. 1996.

7. Scientific Personnel

- Principal Investigator: John F. Doherty, Associate Professor, Penn State University
- Graduate Students
  - J. Yoon, Ph.D., Electrical Engineering, The Pennsylvania State University, In progress
  - J. Wang, Ph.D., Electrical Engineering, The Pennsylvania State University, In progress
  - Y. Hsieh, M.S., Electrical Engineering, The Pennsylvania State University, August 1998
  - J. Koo, M.S., Electrical Engineering, The Pennsylvania State University, August 1998
  - S. C. Park, Ph.D., Electrical Engineering, Iowa State University, December 1996
  - V. Raveendran, M.S., Electrical Engineering, Iowa State University, December 1996

Bibliography

[1] S. Verdu, "Recent Progress in Multiuser Detection," in Multiple Access Communications, IEEE Press, Piscataway, NJ, 1993.

[2] S. Verdu, "Minimum Probability of Error for Asynchronous Gaussian Multiple Access Channels," *IEEE Transactions on Information Theory*, Vol. 32, No.1, pp. 85-96, Jan. 1986.

[3] QUALCOMM, The CDMA Network Engineering Handbook Volume 1: Concepts in CDMA. QUALCOMM Inc., San Diego, CA, February, 1993.

[4] S. Verdu, "Optimum Multiuser Asymptotic Efficiency," *IEEE Transactions on Communications*, Vol. 34, pp. 891-897, Sep. 1986.

[5] R. Lupas and S. Verdu, "Near-Far Resistance of Multiuser Detector in Asynchronous Channels," *IEEE Transactions on Communications*, Vol. 38, No.4, pp. 496-508, Apr. 1990.

[6] R. Lupas and S. Verdu, "Linear Multiuser Detectors for Synchronous Code Division Multiple Access Channels," *IEEE Transactions on Information Theory*, Vol. 35, No.1, pp. 123136, Jan. 1989.

[7] M. Varanasi and B. Aazhang, "Near-Optimum Detection in Synchronous Code Division Multiple Access Systems," *IEEE Transactions on Communications*, Vol. 39, No. 5, pp. 725-736, May 1991.

[8] M. K. Varanasi and B. Aazhang, "Multistage Detection in Asynchronous Code Division Multiple-Access Communications," IEEE Transactions on Communications, Vol. 38, No.4, pp. 509519, Apr. 1990.

[9] A. Duel-Hallen, "Decorrelating Decision-Feedback Multiuser Detector for Synchronous Code Division Multiple Access Channel," IEEE Transactions on Communications, Vol. 41, No. 2, pp. 285-290, Feb. 1993.

[10] A. Duel-Hallen, "Equalizers for Multiple Input/Multiple Output Channels and PAM Systems with Cyclostationary Input Sequences," IEEE Journal on Selected Areas in Communications, Vol.10, NO. 3, pp. 630-639, April 1992.

[11] Z. Xie, R. T. Short, and C. K. Rushforth, "A family of suboptimum detectors for coherent multiuser communications," IEEE Journal on Selected Areas in Communications, Vol. 8, NO.4, pp. 683-690, May 1990.

[12] U. Madhow and M. L. Honig, "MMSE Interference Suppression for Direct-Sequence Spread-Spectrum CDMA," IEEE Transactions on Communications, Vol.42, NO.12, pp. 3178-3188, Dec. 1994.

[13] P. B. Rapajic and B. S. Vucetic, "Adaptive Receiver Structures for Asynchronous CDMA Systems," IEEE Journal on Selected Areas in Communications, Vol.12, No.4, pp. 685-697, May 1994.

[14] S. L. Miller, "An Adaptive Direct-Sequence Code-Division Multiple Access Receiver for Multiuser Interference Rejection," IEEE Transactions on Communications, Vol.43, No.2, pp. 17401754, 1995.

[15] S. Haykin, Blind Deconvolution. Prentice Hall, Inc., Englewood Cliffs, NJ, 1994.

[16] M. Honig, U. Madhow, and S. Verdu, "Blind Adaptive Multiuser Detection," IEEE Transactions on Information Theory, Vol.41, NO.4, pp. 944-960, July 1995.

[17] J. B. Schodorf and D. B. Williams, "A Blind Adaptive Interference Cancellation Scheme for CDMA Systems," Proc. Asilomar Conf. Sig. Sys. and Comp., 1995.

[18] M. Honig, U. Madhow, and S. Verdu, "Blind Adaptive Multiuser Detection," IEEE Transactions on Information Theory, Vol.41, NO.4, pp. 944-960, July 1995

[19] B. Widrow, K. M. Duvall, R. Gooch, and W. C. Newman, "Signal Cancellation Phenomena in Adaptive Antennas: Causes and Cures," IEEE Transactions on Antenna and Propagation Vol. AP-SO, No. 3, pp. 469-478, May 1982

[20] M. Feder, A. V. Oppenheim, and E. Weinstein, "Maximum Likelihood Noise Cancellation Using the EM Algorithm," IEEE Transactions on Acoustics, Speech, and Signal Processing, Vol.37 No.2, pp. 204-216, Feb. 1989

[21] U. Madhow and M. L. Honig, "MMSE Interference Suppression for Direct-Sequence Spread-Spectrum CDMA", *IEEE Trans. on Commun.*, vol. 42, no. 12, pp. 3178–3188, Dec 1994.

[22] P. B. Rapajic and B. S. Vucetic, "Adaptive Receiver Structures for Asynchronous CDMA Systems", *IEEE Journal on Selected Areas in Commun.*, vol. 12, no. 4, pp. 685–697, May 1994.

[23] S. L. Miller, "An Adaptive Direct-Sequence Code-Division Multiple-Access Receiver for Multiuser Interference Rejection", *IEEE Trans. on Commun.*, vol. 43, no. 2/3/4, pp. 1746–1755, Feb/Mar/Apr 1995.

[24] S. Haykin, *Adaptive Filter Theory*, Prentice Hall, Englewood Cliffs, NJ, 1991.

[25] G. W. Stewart and J. Sun, *Matrix Perturbation Theory*, Academic Press, San Diego, CA, 1990.

[26] L. Milstein, "Interference rejection techniques in spread spectrum communications," *Proceedings of the IEEE*, vol. 76, pp. 657–671, June 1988.

[27] L. Milstein, "Interference suppression to aid acquisition in direct-sequence spread-spectrum communication," *IEEE Transactions on Communications*, vol. 36, pp. 1200–1207, November 1988.

[28] R. Mammone, ed., *Computational Methods of Signal Recovery and Recognition.* J. Wiley & Sons, 1992.

[29] L. Milstein and R. Iltis, "Signal processing for interference rejection in spread spectrum communications," *IEEE Acoustics, Speech, and Signal Processing Magazine*, vol. 3, pp. 18–31, April 1986.

[30] F. Takawira and L. Milstein, "Narrowband interference rejection in PN spread spectrum systems using decision feedback filters," in *Proceedings of IEEE Military Communications Conference*, pp. 20.4.1–20.4.5, October 1986.

[31] J. Ketchum and J. Proakis, "Adaptive algorithms for estimating and suppressing narrowband interference in PN spread spectrum systems," *IEEE Transactions on Communications*, vol. COM-30, pp. 913–923, May 1982.

[32] R. Iltis and L. Milstein, "An approximate statistical analysis of the widrow LMS algorithm with application to narrow0band interference rejection," *IEEE Transactions on Communications*, vol. COM-33, February 1985.

[33] F. Hsu and A. Giordano, "Digital whitening techniques for improving spread spectrum communications performance in the presence of narrowband jamming and interference," *IEEE Transactions on Communications*, vol. COM-26, 1978.

[34] L. Li and L. Milstein, "Rejection of narrow-band interference in PN spread spectrum systems using transversal filters," *IEEE Transactions on Communications*, vol. COM-30, May 1982.

[35] G. Saulnier, K. Yum, and P. Das, "The suppression of tone jammers using adaptive lattice filtering," in *Proceedings of the IEEE International Conference on Communications*, June 1987.

[36] L. Milstein and P. Das, "An analysis of real-time transform domain filtering digital communication system, part i: Narrowband interference rejection," *IEEE Transactions on Communications*, vol. COM-28, pp. 816–824, June 1980.

[37] I. Howitt, J. Reed, V. Vemuri, and T. Hsia, "Recent developments in applying neural nets to equalization and interference rejection," in *Wireless Personal Communications: Trends and Challenges* (T. Rappaport, B. Woerner, and J. Reed, eds.), Kluwer Academic Publishers, 1994.

[38] J. Doherty, *Direct sequence spread spectrum interference rejection using vector space projection techniques*, ch. 6, pp. 59–67. Kluwer Academic Publishers, 1994.

[39] R. Vijayan and H. Poor, "Nonlinear techniques for interference suppression in spread spectrum systems," *IEEE Transactions on Communications*, vol. COM-38, pp. 1060–1065, July 1991.

[40] J. Doherty, "Linearly constrained direct sequence spread spectrum interference rejection," *IEEE Transactions on Communications*, vol. 42, March 1994.

[41] S. Haykin, *Adaptive Filter Theory.* Prentice-Hall, 2nd ed., 1990.

[42] J. Ortega, *Matrix Theory : A Second Course.* Plenum Press, 1987.

[43] R. L. Pickholtz, D. L. Schilling, and L. B. Milstein, Theory of Spread Spectrum Communications A Tutorial, IEEE Transactions on Communications, Vol. COM-30, No. 5, May 1982.

[44] J. D. Laster and J. H. Reed, Interference Rejection in Digital Wireless Communications, IEEE Signal Processing Magazine, Vol. 14, No. 3, pp.37-62, May 1997.

[45] B. Widrow and S. D. Stearns, Adaptive Signal Processing, Prentice Hall, Englewood Clifts, NJ, 1985.

[46] J.F. Doherty and R.J. Mammone, A Fast Method for Regularized Adaptive Filtering, Digital Signal Processing: A Review Journal, Academic Press, Vol. 2, No. 1, pp. 14-26, January 1992.

[47] J. W. Ketchum and J. G. Proakis, Adaptive Algorithms for Estimating and Suppressing Narrow-Band Intereference in PN Spread-Spectrum Systems, IEEE Transactions on Communications, Vol. COM-30, No. 5, pp. 913-924, May 1982.

[48] M. C. Jeruchim, P. Balaban and K. S. Shanmugan, *Simulation of Communications Systems,* (Plenum Press, New York, 1992).

[49] MATLAB, *SIMULINK Manual,* The Mathworks Inc., (Waltham, MA, 1995).

[50] D. Molkdar and P. A. Matthews, Measurements and Characterization of the UHF Mobile Radio Channel, *J. IRE, Vol. 58, no. 6 (Supplement),* (Sept.-Dec., 1988), S145-S168.

[51] J. G. Proakis, *Digital Communications,* (McGraw-Hill, New York, 1995).

[52] TIA/EIA/IS-95, *Mobile Station-Base Station Compatibility Standard for Dual-Mode Wideband Spread Spectrum Cellular System,* Telecommunication Industry Association, July 1993.

[53] A. M. D. Turkmani, J. D. Parsons, J. Feng and D. G. Lewis, Microcellular Radio Measurements at 900, 1500 and 1800 MHz, *IEE 5th Int. Conf. on Land Mobile Radio,* IEE Conf. Publ. 315, (Warwick, 1989), 65-68